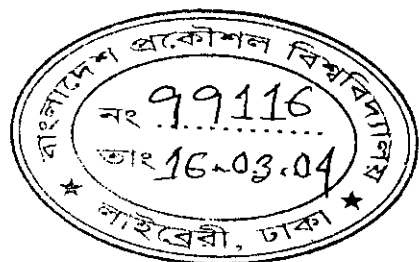# A Study on Heterojunction Structures for High Efficiency Solar Cells

by

Akeed Ahmed Pavel

A thesis

Submitted to the Department of Electrical and Electronic Engineering

in partial fulfillment of the requirements for the degree

of

MASTER OF SCIENCE IN ELECTRICAL AND ELECTRONIC

ENGINEERING

DEPARTMENT OF ELECTRICAL AND ELECTRONIC ENGINEERING

BANGLADESH UNIVERSITY OF ENGINEERING AND TECHNOLOGY

January 2004

The thesis titled, "**A Study on Heterojunction Structures for High Efficiency Solar Cells**," submitted by Akeed Ahmed Pavel, Roll No. 100106253P, Session October-2001 has been accepted as satisfactory in partial fulfillment of the requirements for the degree of **Master of Science in Electrical and Electronic Engineering** on 31st January 2004.
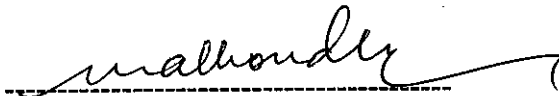
BOARD OF EXAMINERS

1.

Dr. M. Rezwan Khan   Chairman
Professor   (Supervisor)
Department of Electrical and Electronic Engineering
BUET, Dhaka-1000.

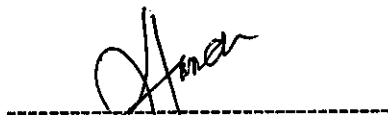2.

Dr. Mohammad Ali Choudhury   Member
Professor and Head   (Ex-Officio)
Department of Electrical and Electronic Engineering
BUET, Dhaka-1000.

3.

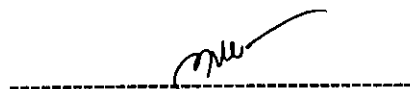**Dr. M. M. Shahidul Hassan**   Member
Professor
Department of Electrical and Electronic Engineering
BUET, Dhaka-1000.

4.

Dr. Md. Abu Hasan Bhuiyan   Member
Professor   (External)
Department of Physics
BUET, Dhaka-1000.

DECLARATION

I hereby declare that this thesis has been completed by me and it or any part of it has not been submitted elsewhere for award of any degree or diploma.

Countersigned   Signature of the Candidate

_____ 31·1·04   _____ 31.1.04

(Dr. M. Rezwan Khan)   **(Akeed Ahmed Pavel)**
Professor
Department of Electrical and Electronic
Engineering
BUET, Dhaka-1000
BANGLADESH.

CONTENTS

LIST OF FIGURES

VIII

LIST OF TABLES

LIST OF SYMBOLS

a	Cross sectional Area	cm^{-2}
D_n	Diffusion Coefficient for Electrons	cm^2/s
D_p	Diffusion Coefficient for Holes	cm^2/s
E_c	Electron Energy at Conduction Band Edge	eV
E_v	Electron Energy at Valence Band Edge	eV
Eg	Energy Band Gap	eV
E_m	Energy Delivered by each Photon at Maximum Power Point	eV
FF	Fill Factor	
I_{dark}	Dark Current	mA
I_m	Current at Maximum Power Point	mA
I_s	Diode Saturation Current	mA
I_{SC}	Short Circuit Current	mA
J_n	Electron Component of Dark Current Density	mA/cm^2
J_{ns}	Electron Component of Dark Saturation Current Density	mA/cm^2
J_{ps}	Hole Component of Dark Saturation Current Density	mA/cm^2
J_p	Hole Component of Dark Current Density	mA/cm^2
K	Boltzmann's Constant	eV/K
L_n	Diffusion Length for Electrons	cm
L_p	Diffusion Length for Holes	cm
N_A	Acceptor Doping Density	cm^{-3}
N_c	Effective Density of States in Conduction Band	cm^{-3}
N_D	Donor Doping Density	cm^{-3}
n_i	Intrinsic Carrier Concentration	cm^{-3}
n_{ph}	Number of Photons	$cm^{-2}s^{-1}$
n_{po}	Equilibrium Electron Concentration in p-type material	cm^{-3}
n_s	Number of Photons per unit Volume at a Particular Energy	$cm^{-3}eV^{-3}$
N_v	Effective Density of States in Valence Band	cm^{-3}
P	Power	W

P_{in}	Input Power	W
P_m	Maximum Output Power of Solar Cell	W
P_{no}	Equilibrium Hole Concentration in n-type material	cm^{-3}
q	Electronic Charge	C
QE	Quantum Efficiency	
T	Absolute Temperature	K
V_d	Built in Potential	V
V_m	Voltage Corresponding to Maximum output Power	V
V_{oc}	Open Circuit Voltage	V
w	Width	cm
ΔE_C	Discontinuity between Conduction Bands of a heterojunction	eV
ΔE_V	Discontinuity between Valence Bands of a heterojunction	eV
η	Efficiency	
μ_n	Mobility of Electrons	cm^{-2}/V-s
μ_p	Mobility of Holes	cm^{-2}/V-s

ABSTRACT

In this thesis, the main inherent reasons behind the low conversion efficiency of *p-n* junction solar cells have been studied. The *p-n* junction solar cells are sensitive only to photons with quantum energy higher than the band gap of the material from which they are made. The conversion efficiency of such cells are limited by the fact that the ratio of output work to input photon energy becomes maximum only for the photons having energy close to the band gap of the material. The efficiency of *p-n* junction solar cells is also reduced due to reduction in junction potential barrier under illuminated condition, which causes an enhanced rate of internal recombination of the photo generated carriers. Prevention of internal recombination of electron hole pairs under illuminated condition seems to be a solution towards the enhancement of the cell efficiency. In this work, the mechanism of electron-hole recombination in illuminated *p-n* junction solar cells have been studied. It has been shown here that the value of density of states and mobility difference between electrons and holes have significant impact on the mechanism of internal recombination of photogenerated carriers and cell efficiency. Accordingly, some potential heterojunction structures have been proposed that can effectively prevent the high rate of such recombination. Results presented here indicate that significant improvement in cell efficiency can be achieved by using these proposed structure.

CHAPTER 1

INTRODUCTION
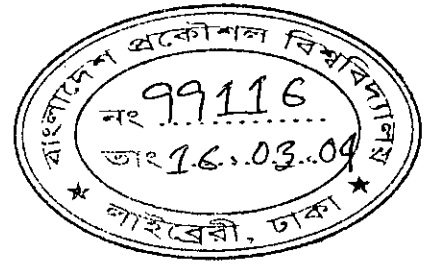
1.1 Background and Present State of the Problem

Due to worldwide ever-increasing demand for energy, the conventional energy resources, such as fossil fuels are going to be exhausted in not-too-distant future. Therefore, technology must be developed to extract energy from non-exhaustible natural sources. Solar cell is one of the most promising candidates for obtaining energy from our only long-term natural resource, the sun.

Solar cells are not at all new: Rather some of the earliest semiconductor devices, including first thin-film selenium cell developed from 1880, were solar cells [1]. However, these early devices which became popular around 1930 [1], were not efficient enough for power generation and was mainly used as large area photodetectors. The evolution of crystalline silicon technology in the 1950s made possible the first practical energy conversion applications and in consequence silicon solar cells was first developed using diffused *p-n* junction in 1954 [2]. But these cells were too expensive for general use. However, the use of solar cells in spacecrafts from late 1950s established a small industry supplying space cells. Later many companies began specializing in the production of solar cells for terrestrial purpose, primarily for telecommunications and similar applications involving small "remote" electrical loads such as navigational aid [3]. The cost of these terrestrial cells has decreased significantly over the last two decades due to increased manufacturing volume and improved processing techniques.

But the main problem still associated with solar cells is their low conversion efficiency. One of the fundamental limitations on solar cell efficiency is the bandgap of the semiconductors from which the cell is made. As solar cells respond only to those photons that have energy greater than the band gap of its material, a considerable part of the solar radiation remains unabsorbed. Another reason for low efficiency is the internal

recombination of the excess charge carriers generated by photon absorption. As a result, fewer charge carriers remain available for flowing through the external load. These two unwanted phenomena lead to lower values of 'short circuit current' and 'open circuit voltage' respectively, which, we will see in later chapters, are two key factors for increasing solar cell efficiency. In case of single material homojunction solar cell, the spectral response or short circuit current can be increased by choosing semiconductors with lower band gap. But such a choice would increase the rate of internal recombination of the excess charge carriers leading to lower open circuit voltage. Theoretically, the highest efficiency for such solar cells made from a single material has been found to be 31% for an energy band gap of around 1.35 eV [4]. But, experimentally, the maximum conversion efficiency of a single homo-junction solar cell, under concentration of 1 sun condition, has been reported to be around 25% [5-6]. However, the efficiencies of commercially available solar cells are even lower, around 15% only [6]. Stacking of different band gap materials in multi junction cells to catch photons of almost all energies can achieve the maximum theoretical efficiencies of 37%, 50%, 56% and 72 % for 1,2,3 and 36 energy gaps respectively, at a concentration of 1000 sun [7]. But too many practical problems, including mismatch in cascaded cells and difficulty in fabrication, intervene with such cells which makes it virtually impossible to achieve the ultimate efficiency of 72% in reality. However, it has been found experimentally that the most efficient multijunction cell has just two layers with efficiency around only 30% [5]. That is why, enhancement of solar cell efficiency is a topic of ongoing research and several attempts are being made to achieve higher conversion efficiency using different materials and structures.

With the advancement of semiconductor device technology, several silicon *p-n* junction configurations with simpler structures have been proposed to alleviate the detrimental effects of poor spectral response and high rate of internal recombination. In 1972, "back surface field (BSF)" silicon solar cells was developed that introduced the concept of shielding photogenerated excess minority carriers from internal recombination by employing the electric field of low-high junction [8-9]. During the time Si *p-n* junction solar cells were entering this period of innovations, some other homojunction

configurations in other semiconductors like a shallow GaAs homojunction cell with 20% efficiency was demonstrated [9-10]. The 'heteroface' solar cell, which is a GaAs p-n homojunction with an added layer of high band gap $Al_xGa_{1-x}As$, was also introduced in 1973 [11]. The conversion efficiency of the 'heteroface' solar cell having p-$Ga_{1-x}Al_xAs/p$-$GaAs/n$-$GaAs$ structure has been reported to be more than 22% [11-12]. In this structure the high band gap p-$Ga_{1-x}Al_xAs$ layer has been used to reduce the rate of internal recombination and lower band gap GaAs p-n junction has been used for absorbing photons at relatively low energy. A GaAs solar cell with 26.2% efficiency has been demonstrated that employs the technique of concentrating sunlight on the cell with added cost of the concentrator [13].

Beside the above mentioned p-n junctions, several other structures, including MIS (metal-insulator-semiconductor), schottky barriers, heterojunctions and grating cells have been proposed with unique advantages of one kind or another [14]. MIS inversion layer solar cells have shown good promise regarding efficiency [15]. Schottky barrier solar cells, although has improved spectral response, their efficiencies are some what lower due to lower open circuit voltage [14]. Heterojunction solar cells, on the other hand, have higher potential regarding efficiency, as it is possible to improve both the spectral response and open circuit voltage using such structures [14,16]. Heterojunction cells are also very promising for terrestrial use for their low cost and easy fabrication [14].

Except Si and GaAs, use of several compound semiconductor materials, such as cadmium telluriaum (CdTe) [17], cadmium sulphide (CdS) [18], indium nitride (InN) [19] etc. have been proposed for achieving higher conversion efficiency and reduced cost. Finally, in very recent time, it has been shown that enhancement of ideal solar cell efficiency can be achieved by photonic excitations in multi-intermediate band structures provided that technology for electronic band gap engineering is available [20]. Although with these efforts, the problem regarding low solar cell efficiency and high cost has been alleviated to some extent, there is still a lot of room for further improvement.

1.2 Objective of the Thesis

The objective of this thesis is to analyze the reasons behind the low conversion efficiency of the existing solar cells and to propose some new heterojunction structures for improving the scenario. The single junction solar cell properties has been studied first to understand the individual contributions of some device parameters like mobility, density of states, diffusion length etc. in limiting the solar cell efficiency. Based on such focused study on the above-mentioned parameters, this work proposes some potential heterostructures that can exploit those parameters for achieving higher conversion efficiency.

1.3 Thesis Outline

The conversion efficiency of a solar cell can be defined as a measure of work done per photon. Increasing the efficiency is essentially a matter of increasing the ratio of work extracted to photon energy supplied. This thesis is concerned with identifying the underlying reasons for low efficiency and proposing some potential structures for higher efficiency.

In the following chapter (chapter 2), the basic principle of photovoltaic energy conversion by a p-n homojunction and the performance characteristics of a solar cell has been reviewed first. The efficiency calculation of a typical p-n homojunction solar cell has also been presented in very brief, followed by a discussion identifying the main reasons behind their low efficiency. Finally, the strategies for achieving higher cell efficiency proposed in this work has been outlined.

In chapter three, the current-voltage (I-V) characteristics of a typical heterojunction solar cell under illumination has been presented. From these characteristics, the factors influencing the conversion efficiency are identified. It has been shown that, so far the reported works have not given due consideration to some of the very important semiconductor parameters, like mobility and density of states, that plays very significant

role in determining the overall cell efficiency. A comparative analysis among several heterojunction configurations has been presented next, to hi-light the importance of those parameters in designing single junction heterostructure solar cell with higher efficiency.

Some new heterojunction structures having potential for even higher conversion efficiency has been proposed in chapter four. These structures are modified versions of 'heteroface' solar cell [11-12]. Here also, the I-V characteristics of these solar cells under illumination have been presented. It has been shown that careful choice of the parameters discussed in chapter 2 can lead to the considerable enhancement of efficiency over the reported efficiency of heteroface cell [11-12].

The concluding chapter (chapter 5) provides a comprehensive summary of the whole work followed by a brief discussion on limitations of this work and some suggestions for future work.

CHAPTER 2

p-n JUNCTION SOLAR CELLS

2.1 Introduction

In their most common form, solar cells are large area *p-n* junction diodes specially designed to convert sunlight into electricity. Figure 2.1a schematically shows a typical *p-n* junction solar cell. Photons within the incoming solar radiation that have quantum energy greater than the bandgap of the solar cell material give up their energy by exciting electrons from the valence band to the conduction band of the material. Thus electron-hole pairs (EHP) are created in the cell. These electrons and holes tend to recombine naturally after a finite time. However, the electrons (or holes) generated close to or within the depletion region are pulled away across the junction by its built-in electric field to a neutral region where very few holes (or electrons) are available for recombination. If further recombination is avoided, these charge carriers will reach the terminals or contacts to the cell and will ultimately flow through the external load. This mechanism of charge separation and their direction of flow through the cell imparted by the asymmetric electronic property of the junction have been shown in figure 2.1b.

(a)   (b)
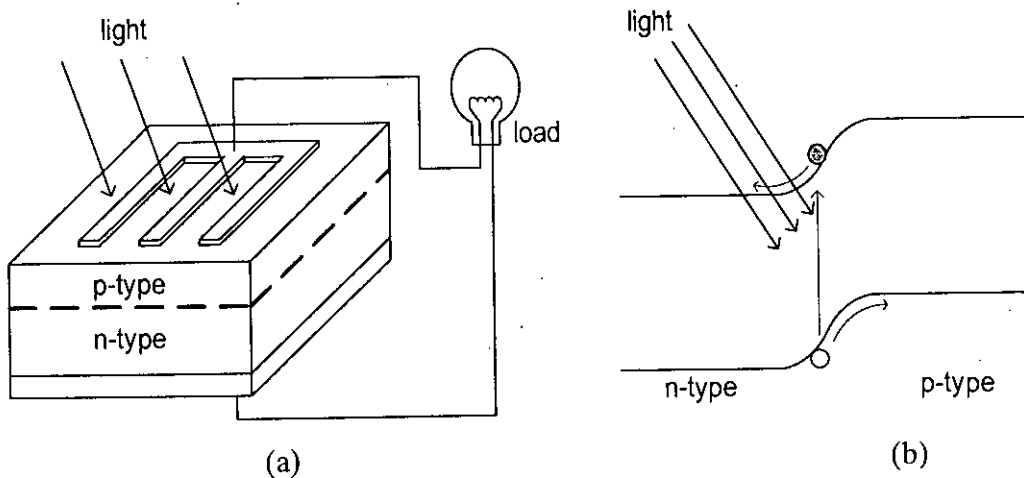
Figure 2.1: (a) A typical *p-n* junction solar cell under illumination. (b) Generation of EHP by solar radiation and charge separation by the built-in electric field.

Due to such charge separation, electrons and holes get accumulated in n and p type materials respectively. This makes the p-n junction forward biased and so the potential barrier is reduced. Consequently some of the photogenerated carriers start to flow in opposite direction overcoming this reduced potential barrier. The carriers, that have been successful to overcome the barrier, ultimately recombines internally within the cell and so are unavailable to flow through the external load. This recombination mechanism, which in fact gives rise to diode current, has been termed as internal recombination.

2.2 Performance Characteristics

2.2.1 Photocurrent and Short Circuit Current

The photo-generated electrons and holes close to and within the depletion region are separated by the asymmetric electronic property of the junction. This mechanism of charge separation also imparts directionality to the flow of these excess charge carriers and some of them become successful to reach the external contacts, avoiding the internal recombination within the cell. The electric current that results from the flow of those successful carriers is termed as *photocurrent* [6]. It depends on the intensity of incident light.

The photocurrent that flows when the terminals of the solar cell are connected together or *'shorted'* is known as *short circuit current* (I_{SC}). The recombination of the carriers under short circuit condition can be neglected. So during such condition, all most all the photogenerated carriers flow through the external load and the rate of internal recombination becomes zero. It depends on the absorption coefficient and current transport efficiency of the cell material through cell's *Quantum Efficiency* (*QE*), which is defined, in this case, as the probability that an incident photon of quantum energy E will deliver one electron to the external circuit. Theoretically, short circuit current density can be expressed as [6]:

$$I_{SC} = q \int n_s(E) QE(E) dE \qquad (2.1)$$

where q is the electronic charge and n_S is the number of photons per unit volume with a particular energy E.

2.2.2 Dark Current and Open Circuit Voltage

Separation of photo-generated charge carriers by the junction potential causes accumulation of electrons and holes on n-side and p-side respectively. This makes an illuminated p-n junction forward biased and normal diode current starts to flow opposing the photocurrent. In case of solar cell this diode current is termed as *dark current* and is given by typical current-voltage $(I$-$V)$ relationship of a p-n junction diode:

$$I_{dark} = I_S (e^{qV/kT}-1) \qquad (2.2)$$

where k is the Boltzmann constant, T is absolute temperature, V is the voltage and I_S is the diode saturation current. The diode saturation current I_S depends on the semiconductor used for making the junction and for p-n homojunction it is given by the following equation:

$$I_S = qN_C N_V \left(\frac{D_n}{L_n N_A} + \frac{D_p}{L_p N_D}\right) e^{-Eg/kT} \qquad (2.3)$$

where E_g is the energy band gap of the cell material, $N_{C,V}$ are the density of states at conduction and valence bands, $D_{n,p}$ are diffusion constants, $L_{n,p}$ are diffusion lengths for electrons and holes respectively.

When the photocurrent is superimposed upon the normal rectifying current-voltage characteristics of the junction expressed by equation 2.2, it is displaced downwards by a certain amount depending on the intensity of light. Under short circuit condition the dark current becomes zero and the photocurrent becomes equal to the short circuit current I_{SC}. The overall current-voltage $(I$-$V)$ characteristics of an illuminated p-n junction is therefore given by

$$I = I_S (e^{qV/kT}-1) - I_L \qquad (2.4)$$

where I_L is the photocurrent.
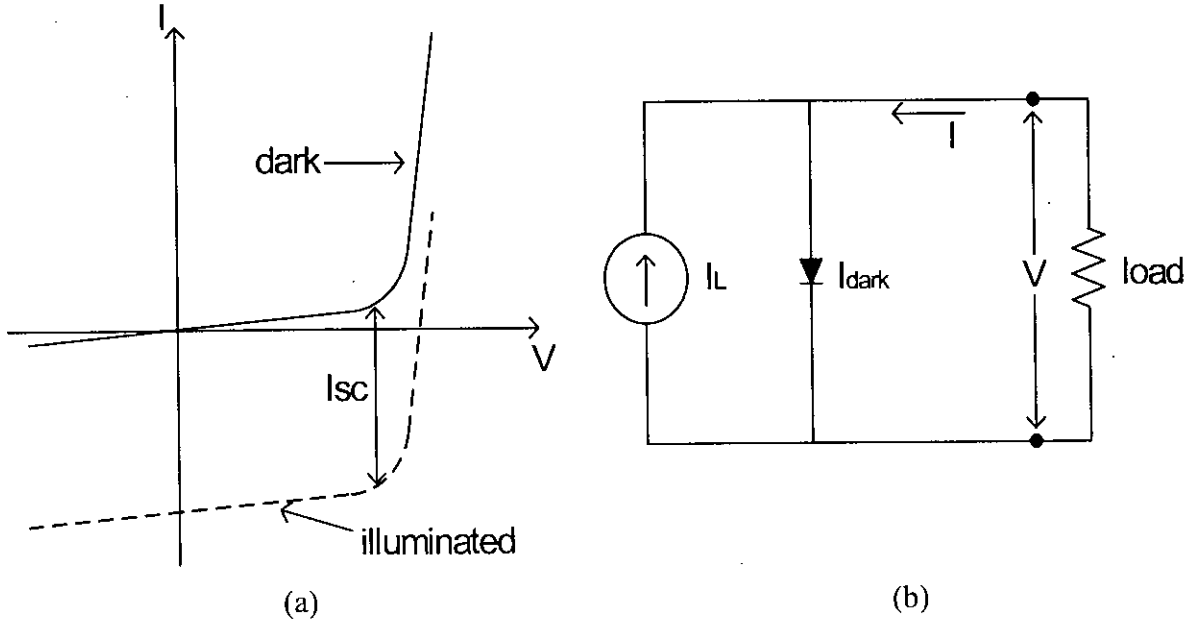
Figure 2.2: (a) I-V characteristics of a p-n junction solar cell in dark (solid line) and under illumination (dashed line). (b) Idealized equivalent circuit of a p-n junction solar cell.

In Figure 2.2, this over all I-V characteristics of an illuminated p-n junction solar cell along with its equivalent circuit have been shown.

The dark current increases exponentially with the voltage across the terminal contacts and reach its maximum value when it becomes equal to the short circuit current. At this condition, all the photo-generated carriers actually cross over the junction barrier and recombine internally leaving no carriers available to flow through the external load. This is equivalent to the condition which would occur if the terminal contacts of the cell were isolated or left open. Of course, the potential difference across the terminal also reaches its maximum value at this condition. This voltage is known as the *open circuit voltage*, V_{OC}. So, the open circuit voltage can be calculated from equation 2.4 by putting dark current equal to short circuit current:

$$V_{OC} = \frac{kT}{q}\ln(1 + \frac{I_L}{I_S})$$

(2.5)

2.2.3 Fill Factor and Efficiency

The solar cell delivers power to the external circuit in it's operating regime. This regime, shown in figure 2.3a, is represented by the portion of the I-V curve given by equation 2.4, that has been forced into the fourth quadrant. As is normal practice, figure 2.3a shows the fourth quadrant region of Fig. 2.2a inverted so that it lies in the first quadrant. The output power $P=IV$, is given by the area of the rectangles corresponding to particular voltages and currents. Figure 2.3 shows output powers corresponding to several voltage and current values. It is clearly seen from the figure that output power reaches its maximum value at some voltage V_m corresponding to current I_m. The maximum power, $V_m I_m$, has been represented by the shaded rectangle in figure 2.3. With reference to figure 2.3, fill factor FF, which describes the squareness of the curve, can be defined as

$$FF = \frac{V_m I_m}{V_{oc} I_{sc}} \qquad (2.6)$$
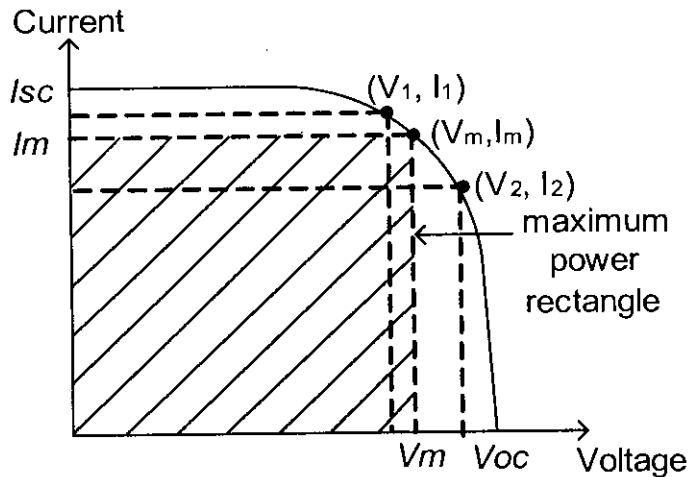
Figure 2.3: I-V characteristics reflected in the voltage axis to bring it into the first quadrant. The shaded area is proportional to the power output of the cell.

The conversion *efficiency* η, of the cell is defined as the ratio of maximum power $(V_m I_m)$ delivered by the cell to the incident photon power P_{in},

$$\eta = \frac{V_m I_m}{P_{in}} \qquad (2.7)$$

The conversion efficiency can be also expressed in terms of V_{OC}, I_{SC} and FF

$$\eta = \frac{V_{OC} I_{SC} . FF}{P_{in}} \qquad (2.8)$$

So, to maximize efficiency, all three quantities in the numerator of equation 2.8 have to be maximized.

All these four quantities: V_{OC}, I_{SC}, FF and η are the key performance characteristics and therefore, should be defined for particular illumination conditions. Performance characteristics for most common cell materials can be found in reference [6].

2.3 Ideal Conversion Efficiency

A variety of approaches have been proposed and developed for calculating the upper limit of the conversion efficiency achievable by photovoltaic process. The most efficient approaches developed to date are based on "detailed balance" between light absorption by the solar cell material and the reverse process of light emission by a forward-biased p-n junction [21,7].

The power output of a p-n junction under illumination, and hence cell conversion efficiency can be calculated in relatively straightforward fashion by using the I-V characteristics shown in fig.2.3 and given by eq. 2.4. The output power is given by

$$P = IV = I_S V (e^{qV/kT}-1) - I_L V \qquad (2.9)$$

The upper limit to the current is the short circuit current (I_{SC}), which is determined by the number of photons in the incident sunlight with sufficient quantum energy to create electron-hole pairs in the active collection region of the cell [3-4]. The upper limit to the voltage is the open circuit voltage given by equation. 2.5. The condition for maximum

output power can be obtained by putting $dP/dV = 0$. The current and voltage at maximum power point can be expressed as:

$$I_m = I_S \beta V_m e^{\beta V_m} \qquad (2.10a)$$

$$V_m = \frac{1}{\beta} \ln\left(\frac{I_L/I_S + 1}{1 + \beta V_m}\right) = V_{OC} - \frac{1}{\beta} \ln(1 + \beta V_m) \qquad (2.10b)$$

where $\beta = q/kT$. So, the maximum power output P_m is given by

$$P_m = I_m V_m = I_L \left[V_{OC} - \frac{1}{\beta} \ln(1 + \beta V_m) - \frac{1}{\beta} \right] = I_L(E_m/q) \qquad (2.11a)$$
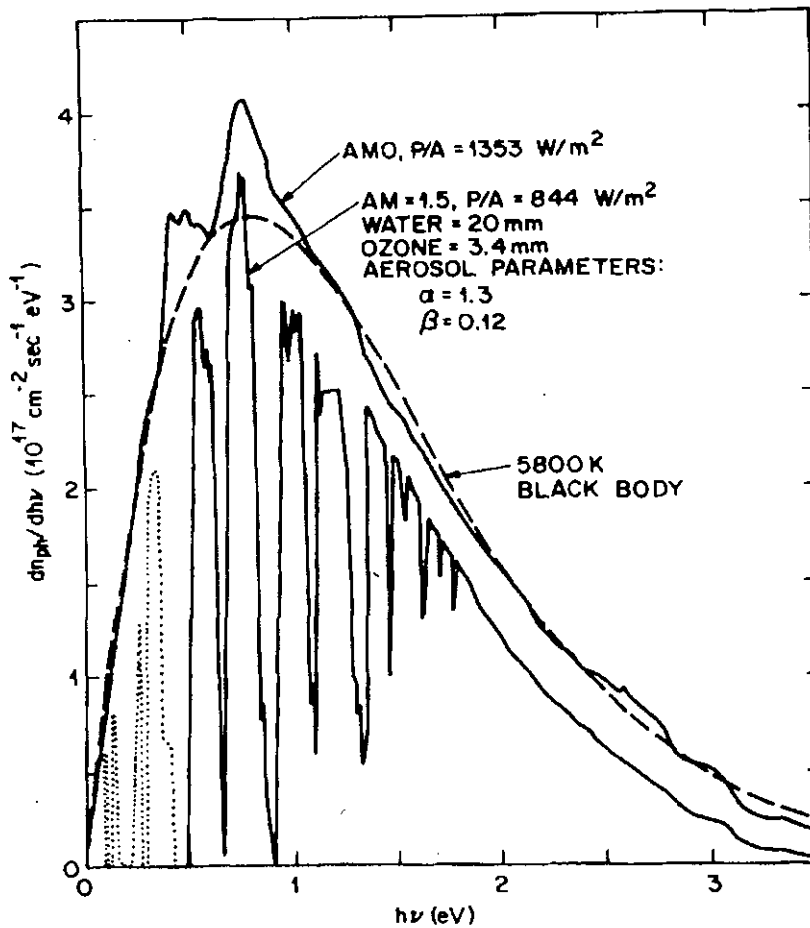
Figure 2.4a: Solar Spectrum as a function of photon energy for AM0 and AM1.5 conditions [7].
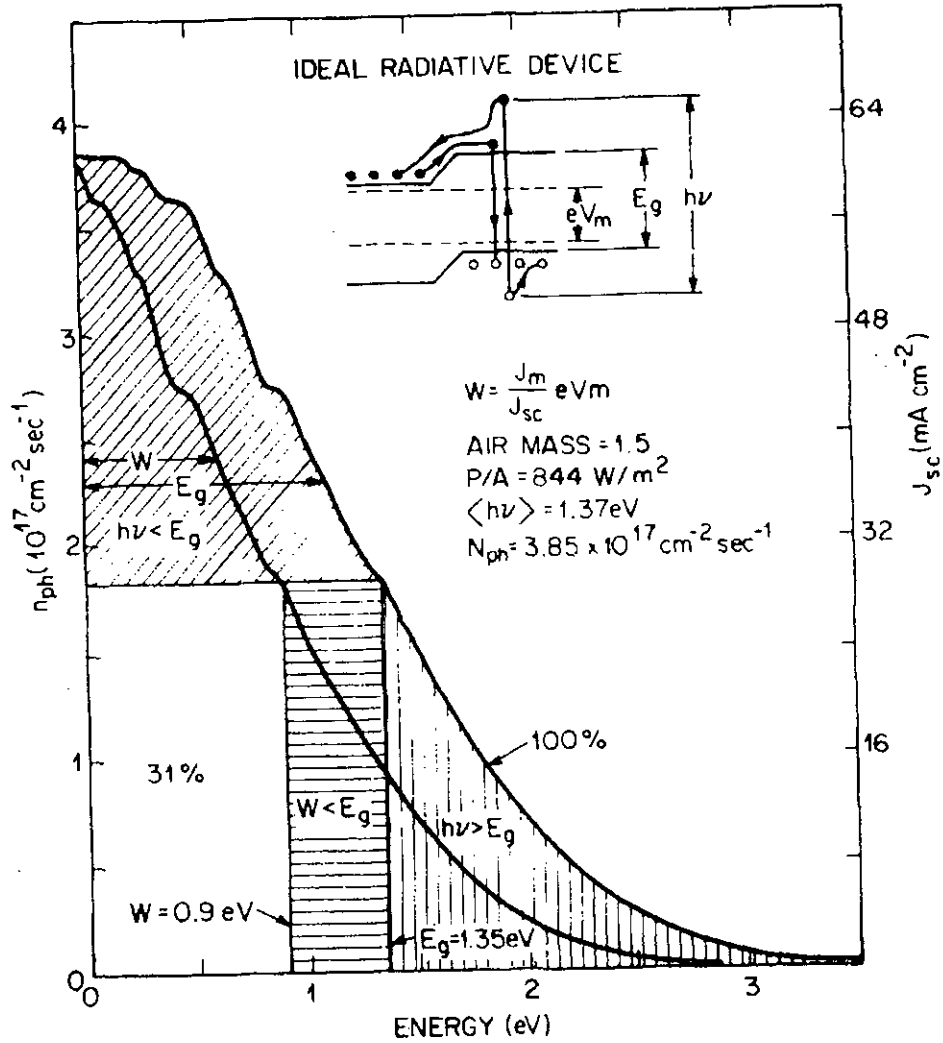
Figure 2.4b: Number of photons in a solar spectrum and corresponding short circuit current as a function of photon energy [7].

where

$$E_m = q[\ V_{OC} - \frac{1}{\beta}\ \ln\ (1+ \beta V_m)- \frac{1}{\beta}\ ] \qquad (2.11b)$$

E_m corresponds to the energy delivered to the load by each photon at the maximum power point.

The short circuit current density (J_{SC}) can be obtained graphically from figure 2.4a [7], assuming that all the photons with quantum energy higher than or equal to the band gap (E_g) of the material will contribute one electron to the external circuit:

$$J_{SC} (E_g) = q \int_{h\nu}^{\infty} \frac{dn_{ph}}{dh\nu} d(h\nu) \qquad (2.12)$$

The result of the integration is shown in the outer curve of figure 2.4b. With the values of J_S and J_{SC} known, P_m can be obtained by numerical solution of eqs. 2.5, 2.9 and 2.10 [4].

It is seen from the above equations (2.9-2.10), that the maximum power output is very much dependent on the "knee" voltage or V_m of the illuminated p-n junction diode, which, in turn depends on the 'dark' saturation current I_S. So one of the key questions in calculating conversion efficiency limit is how small this saturation current can become. For a given semiconductor, this saturation current density given by eq. 2.3, is determined by the diode geometry and other design and material parameters such as doping level and surface recombination velocities [3-4].

The conversion efficiency, which is the ratio of the maximum power output to the incident power P_{in}, can be expressed by the following equation [4]

$$\eta = \frac{P_m}{P_{in}} = \frac{V_m^2 I_S (q/kT) e^{qVm/kT}}{P_{in}} \qquad (2.13)$$

where P_{in} is given by the area under the outer curve of figure 2.4b.

The efficiency can be also obtained graphically from figure 2.4b as described in reference [7]. The maximum efficiency of a single p-n homojunction under the concentration of 1 sun, found by this graphical method is 31% for E_g=1.35 eV using the material parameters corresponding to III-V semiconductors. This 1.35 eV energy band gap is very close to the band gaps of InP (1.34eV) and GaAs (1.42 eV). Under 1000 sun concentration this efficiency improves up to 37% for similar band gap materials [4].

14

2.4 Limiting Efficiency of a Solar Cell

The maximum limit on efficiency imposed by thermodynamics for the direct conversion of solar radiation into work is 93% [7]. But the efficiency of an ideal solar cell is even limited by some intrinsic losses. The first of these losses is due to the inability of a single energy gap solar cell to properly match the broad solar spectrum, which leads to poor spectral response and short circuit current. The photons with quantum energy less than the energy gap E_g are not absorbed at all. The photons with quantum energy greater than the band gap, on the other hand, generates electron-hole pairs which immediately loose almost all energy excess to E_g by thermal dissipation, as shown by figure 2.5. The second intrinsic loss is due to radiative recombination. In this process, a photon creates an electron-hole pair, which recombines radiatively [3,22]. The rate of radiative recombination increases exponentially with the voltage developed across the load. The
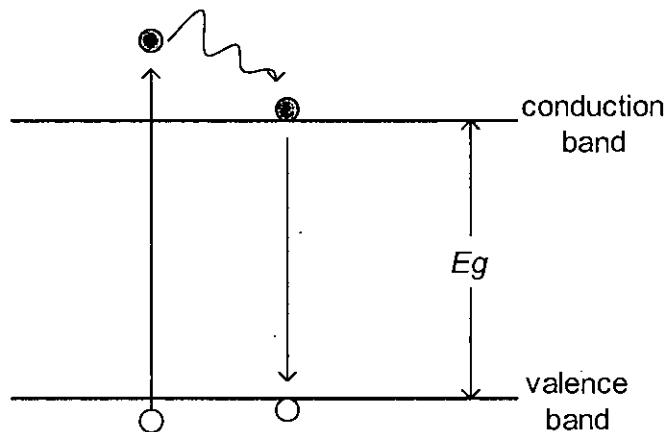
Figure 2.5: Loss of energy as heat due to the absorption of photon with quantum energy higher than E_g.

current due to radiative recombination has direction opposite to that of the current delivered to external load by the cell [7]. The approach of efficiency calculation considering the above two intrinsic losses and using the principle of 'detailed balance' was proposed by Shocley and Queisser [21]. The maximum theoretical efficiency predicted by this approach is 31% for single gap and 72% for 36 cascaded energy gap ideal cells under 1 sun intensity. This 72% efficiency, which is achieved by matching

almost the entire solar spectrum, is still less than the thermodynamic limit of 93% because of radiative recombination. However, the theoretical limit of 72% efficiency is not achievable in reality because numerous practical problems are associated with such multi-energy gap solar cells, including lattice mismatch among the materials of cells to be connected in tandem.

In case of real material systems for photovoltaic conversion, the detail balance limit of 31% efficiency for a single gap ideal cell is also not achievable. This is because of (i) poor spectral response or failure to absorb all of the incident light; (ii) loss of some charges through non radiative recombination of photo-generated excess carriers; (iii) loss of voltage through series resistance. That is why the highest practical efficiency achieved by a single junction cell has been reported to be 25% [5]. For a single p-n junction cell, it is possible to improve the spectral response and hence short circuit current by choosing material with smaller band gap. But such a choice will increase the rate of non-radiative recombination of the excess charge carriers, which will in turn reduce the open circuit voltage and efficiency. So there is an optimum band gap for maximum conversion efficiency and that is predicted to lie around 1.35 eV [23], which is close to the band gap of InP and GaAs. Indeed, the most efficient single junction cell fabricated till to date have been based on GaAs, with efficiencies around 25% [3,5].

2.5 Achieving Higher Conversion Efficiency

The main reasons of the efficiency of a practical single junction solar cell falling behind the 'detail balance limit' are internal non-radiative recombination of photo-generated charge carriers and poor spectral response due to the failure of the cell material to absorb a considerable part of solar spectrum.

As the inherent potential barriers of a p-n junction separates the photo-generated electron-hole pairs, the junction becomes forward biased due to accumulation of charges on either sides of the junction (electrons on n-side and holes on p-side, as shown in figure 2.1b). This causes a reduction in the potential barrier. Assuming that holes and electrons are in
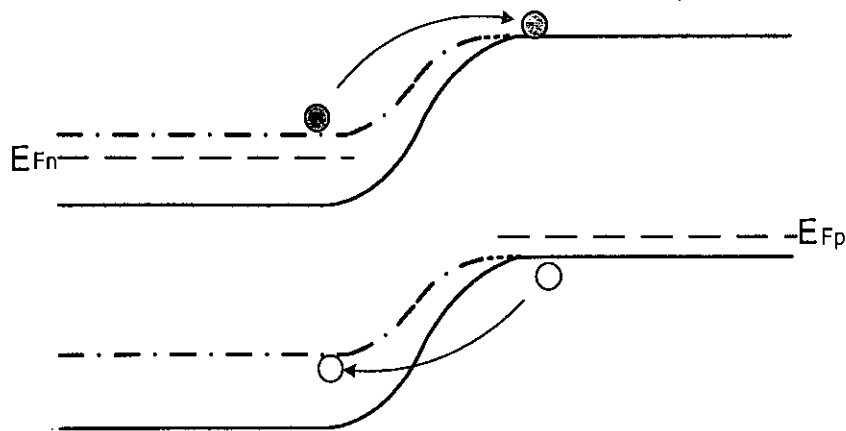
Figure 2.6: Energy band diagram of a *p-n* junction. The firm lines represent the band edges at equilibrium and where as dotted lines represent the band edges under illuminating condition. The quasi-Fermi levels for electrons and holes are also shown.

quasi-thermal equilibrium, there are always significant number of electrons and holes that can cross over this reduced potential hill and cause an internal current flow by drift-diffusion mechanism. This current is similar to normal diode current and so increases exponentially with the voltage developed across the cell under illumination. The potential barrier cross over mechanism has been depicted in Fig 2.6, where the dotted lines show the energy band diagram of a forward biased *p-n* junction due to illumination. Under open circuit condition, photo generated electron and hole pairs keep on accumulating and the internal diode current starts flowing. The internal recombination current keeps on increasing until the cell reaches its open circuit voltage when all the optically generated electrons and holes cross over the barrier and recombine. Any mechanism that can discourage such diffusion across the *p-n* junction would effectively reduce internal recombination and consequentially would increase open circuit voltage. Such a mechanism that can increase the open circuit voltage without causing any significant reduction in the short circuit current would ultimately increase the overall conversion efficiency. Practically, *p-n* junctions formed by higher band gap materials offer higher potential barriers to the charge carriers at the expense of reduced short circuit current. Because as the band gap is increased, the short circuit is reduced, as lesser number of photons would have sufficient energy to generate electron hole pairs. Hence, any

indefinite increase in the band gap ultimately causes reduction of over all cell efficiency. On the other hand, reduction of the band gap increases the short circuit current but reduces the open circuit voltage. Hence, an optimum material band gap that produces maximum conversion efficiency has to be chosen for a homojunction which has been reported to be around 1.35eV [4].

In case of heterojunction structures, it is possible to increase the short circuit current by absorbing wider band of solar spectrum. With heterojunction structures, photons with different range of energies can be absorbed efficiently by different band gap materials involved in forming the junction. It has been explained in the next chapters that higher open circuit voltage can be achieved in case of heterojunction solar cells by offering different potential barriers to electrons and holes. The reported works mainly concentrated on the band gaps of such *p-n* junction structures without giving due consideration to the fact that density of states, mobility difference between electrons and holes can also play very important role in determining the overall efficiency of heterojunction solar cells.

This work makes focused study on the behavior of the above mentioned parameters and suggests some potential heterojunction structures for solar cells that can exploit those parameters for achieving higher conversion efficiency.

CHAPTER 3

p-n HETEROJUNCTION SOLAR CELLS

3.1 Introduction

A heterojunction is formed between two semiconductors having different energy band gaps. The energy band diagrams of two possible p-n heterojunction structures at equilibrium are shown in figure 3.1. Incase of the structure shown in figure 3.1a, n-type material has higher band gap than p-type material. The situation is reversed for the structure shown in figure 3.1b, where p-type material has higher band gap than n-type material. When used as solar cells, light usually enter through the high band gap material and so the structures are known as n-on-p and p-on-n structures respectively. For both the structures, E_{g1} and E_{g2} represents the band gaps of higher band gap and lower band gap materials respectively. Photons with quantum energy higher than E_{g1} are absorbed by the high band gap material. However, photons with energy less than E_{g1} and greater than E_{g2} are passed through the high band gap material and are ultimately absorbed by the lower

(a)   (b)
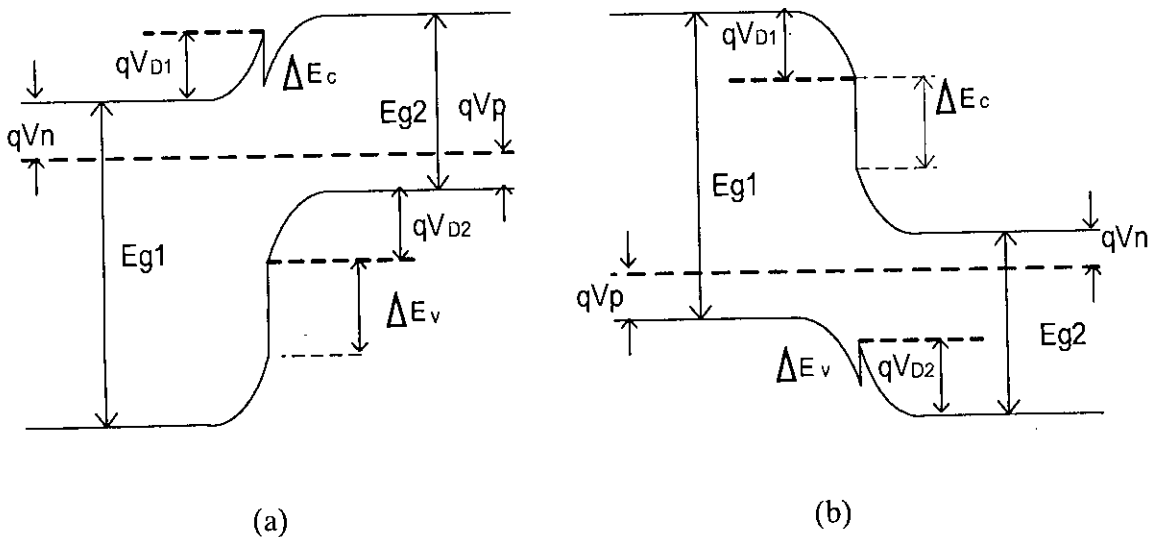
Figure 3.1: Energy band diagrams of p-n heterojunctions (a) with high band gap n type material (n-on-p). (b) high band gap p type material (p-on-n).

band gap material. The carriers generated photonically, in the depletion region or within the diffusion length of the junction, are collected similar to a p-n homojunction solar cell.

As pointed out in the previous chapter, achieving higher open circuit voltage without significant reduction in short circuit current has been a problem for homojunction solar cells. Practically, high band gap materials should be used to form junction with higher built in potential and hence to achieve higher open circuit voltage. But any arbitrary high band gap material can not be chosen for homojunction solar cells, as that would cause considerable reduction of short circuit current and efficiency. On the other hand if lower band gap material is used for forming homojunction, the photons having energy much higher than the band gap loses their excess energy as heat. In fact, the ratio of output work to input photon energy becomes maximum for the photons having energy close to the band gap of the material; for photons having energy less than the band gap it is zero and for photons with energy much higher than the band gap it is very small [6]. In case of heterojunction solar cells, however, this problem can be avoided at least to some extent. The lower band gap material can absorb the photons with low energy and higher band gap material can absorb the high energy photons. Thus heterojunction solar cells can exploit its two different energy gap materials to catch a much wider band of solar radiation efficiently. So heterojunction cells have better spectral response leading to higher short circuit current, as compared to homojunction cells. The other advantages of heterojunction solar cells over conventional p-n homojunction solar cells are (1) lower series resistance and so lower voltage drop, provided that the larger band gap material can be heavily doped without affecting its optical transmission characteristics considerably, (2) high radiation tolerance, provided that the high band gap material is sufficiently thick [4].

Unlike homojunction, a hetero-junction solar cell has unequal potential barriers for holes and electrons and so current in a heterojunction, in most cases, is carried predominantly by either electrons or holes. As shown in figure 3.1a, the potential barrier for holes are much higher than that for electrons. In Fig. 3.1b, however, the situation is just the reverse. Choice between these two possible structures for solar cell is made based on the

open circuit voltage achieved by them. It has been shown later in this chapter that, the dark saturation current, which is determined by the rate of internal recombination, depends on the mobility of charge carriers. Hence, as the mobility of electrons are significantly higher than that of holes, structures having higher potential barrier for the electrons are expected to have higher open circuit voltage. However, there are other factors like density of states, which also play important role in determining the open circuit voltage and all these factors should be incorporated to reach a final conclusion. This chapter presents detailed mathematical analysis that high lights the importance in choosing p-n heterojunction structure for achieving high open circuit voltage.

3.2 Analysis of p-n Heterojunction Solar Cells for Higher Open Circuit Voltage

Typical heterojunction structures are shown in Fig.3.1. Due to difference in the work functions of two different materials, there appears some notch like potential discontinuities in the structure. For the sake of easy understanding and analysis, we have ignored the notch like discontinuity in the following analysis for the structures shown in Fig.3.1a and Fig.3.1b. This notch like discontinuity can be avoided practically by choosing materials with appropriate electron and hole affinity [9].

In the following calculations for the a p-n heterojunction, it have been assumed
a. All the incident photon with energy higher than the smaller band gap is absorbed to produce the short circuit current
b. Potential notches and tunneling effects are negligible
c. Internal resistance has not been considered in the calculation

3.2.1 Dark Current

The variation of dark current with the voltage developed across the p-n heterojunction solar cells, can be expressed as [24]

$$I = Ae^{-qV_{B1}/kT} - Be^{-qV_{B2}/kT}$$ (3.1)

where V_{B1} is the barrier that carriers in semiconductor 1 (with higher band gap) must overcome to reach semiconductor 2 (with smaller band gap), V_{B2} is the barriers for carriers moving in the opposite direction, as shown in figure 3.1. In figure 3.1 and also in the following analysis, material 1 and material 2 represents the materials with higher and lower band gaps (E_{g1} and E_{g2}) respectively. The coefficients A and B are determined by doping levels, carrier effective mass and the mechanism of current flow [24].

In case of heterojunction, due to unequal potential barriers, current is carried out almost entirely by electrons or by holes. For the structure shown in figure 3.1a electrons are the predominant current carrier, whereas holes are the predominant current carriers for the structure shown in figure 3.1b. For the junctions under consideration, both V_{B1} and V_{B2} exist for only the predominant current carriers and so [24]

$$I = A e^{-qV_{D1}/kT} \left(e^{qV_1/kT} - e^{-qV_2/kT} \right) \tag{3.2}$$

where V_1 and V_2 are the portions of voltage developed across material 1 and 2 respectively. However, it should be noted that, for the structures shown in figure 3.1a and 3.1b, $qV_{D2} > \Delta E_C$ and $qV_{D2} > \Delta E_V$ respectively. So, $V_{B2} = 0$ for the respective predominant current carriers and the entire applied voltage is effective in varying the barrier height. The current-voltage relation, considering only the predominant current carriers, is then given by [24]

$$I = A e^{-(qV_D - \Delta E_C)/kT} \left(e^{qV/kT} - 1 \right) \tag{3.3}$$

where V_D is the sum of the partial built in voltages V_{D1} and V_{D2}, supported by two materials at equilibrium (see fig. 3.1). In case of p-n heterojunction, the coefficient A is limited by the rate at which the predominant current carriers (electrons incase of fig 3.1a and holes incase of fig. 3.1b) can diffuse in the narrow band gap material [24],

$$A = a\, q\, X N_{A,D} (D_{n,p}/\tau_{n,p})^{1/2} \tag{3.4}$$

where X is represents the fraction of those carriers having sufficient energy to cross the barrier which actually do so. $N_{A,D}$ is either acceptor or donor doping density in wide band

gap material, a is the cross sectional area of the junction, $D_{n,p}$ is diffusion coefficient and $\tau_{n,p}$ is life times of either electron or hole in the narrow band gap material.

Although, it has been assumed in previous expressions that dark current is entirely dominated by either electrons or holes, dark current that flows inside an illuminated p-n junction obviously has two different components

i. internal current due to the electrons crossing over from the n to p-type material and recombining there (I_n) and

ii. internal current due to holes crossing over from the p to n-type material and recombining there (I_p).

According to equation 3.2 and 3.3, the expressions for electron and hole components of dark current density for the structures shown in fig. 3.1a, can be expressed as

$$J_n = \frac{qD_{n2}}{L_{n2}} N_{D1} e^{-(qV_D - \Delta E_C)/kT} (e^{qV/kT} - 1) \tag{3.4a}$$

$$J_p = \frac{qD_{p1}}{L_{p1}} N_{A2} e^{-(qV_D + \Delta E_V)/kT} (e^{qV/kT} - 1) \tag{3.4b}$$

where $L_{n2,p1}$ are the diffusion lengths for electrons and holes in material 2 and 1 respectively, as shown in figure 3.1, and is given by the following expression:

$$L_{n,p} = (D_{n,p} \tau_{n,p})^{1/2} \tag{3.5}$$

Similarly, the expressions for electron and hole component of dark current density for the structure shown in fig. 3.1b, are given by

$$J_n = \frac{qD_{n1}}{L_{n1}} N_{D2} e^{-(qV_D + \Delta E_C)/kT} (e^{qV/kT} - 1) \tag{3.6a}$$

$$J_p = \frac{qD_{p2}}{L_{p2}} N_{A1} e^{-(qV_D - \Delta E_V)/kT} (e^{qV/kT} - 1) \tag{3.6b}$$

From equation 3.4 and 3.6, it is quite clear that in case of n-on-p structure (fig 3.1a), the dark current is dominated by electrons and in case of p-on-n structure (fig 3.1b), it is dominated by holes. In the above expressions for the current density, the effect of mobility ($\mu_{n,p}$) is included in the diffusion constant $D_{n,p}$ according to the Einstein relationship for non-degenerate semiconductors

$$D_{n,p} = \frac{kT}{q}\mu_{n,p} \tag{3.7}$$

Since electrons have higher mobility than that of holes, one might expect that the dark current should be greater for p-on-n structure. But, as revealed by the following section, it is not always true due to the influence of other parameters like density of states on the dark current through the built in potential.

3.2.2 Built in Potential

The built in potential (V_D) for the structures shown in Fig.3.1a can be expressed as

$$qV_D = E_{g1} - E_V - (qV_n + qV_P) = E_{g2} - (qV_n + qV_P) \tag{3.8}$$

where $qV_{n,p}$ represents the energy difference from the equilibrium Fermi level to the conduction band edge and valence band edge respectively. For non-degenerate semiconductors where Fermi level lies several kT below the conduction band edge, electron density at conduction band edge is given by [25]

$$n = N_C\, e^{-qV_n/kT} \tag{3.9a}$$

Similarly, we can obtain the hole density near the top of valence band [25]:

$$p = N_V\, e^{-qV_p/kT} \tag{3.9b}$$

where $N_{C,V}$ are the density of states at conduction and valence band respectively. Using equation 3.9 and assuming electron and hole density of n and p type material almost

equal to their respective doping density, N_D and N_A, the built in potential can be expressed as:

$$qV_D = E_{g2} - kT \left(\ln \frac{N_{C1}}{N_{D1}} + \ln \frac{N_{V2}}{N_{A2}} \right) \qquad (3.10)$$

$$= E_{g2} + kT \ln \frac{N_{D1}N_{A2}}{N_{C1}N_{V2}} \quad \text{(for the structure shown in fig.3.1a)} \qquad (3.11)$$

where the subscripts 1 and 2 refers to materials with high and low band gap respectively. The expression for built in potential for the structure 3.1b can be obtained similarly and is given by:

$$qV_D = E_{g2} + kT \ln \frac{N_{D2}N_{A1}}{N_{C2}N_{V1}} \quad \text{(for the structure shown in fig.3.1b)} \qquad (3.12)$$

Since for non-degenerate semiconductors $N_A N_D < N_C N_V$ [4], the upper limit of built in potential for both the structures are set by band gap of the low band gap material and so is equal to E_{g2}.

From the above two equations (equation 3.11-3.12), it is quite clear that built in potential can be different due to the variation in the values of N_C and N_V, even if same doping densities are used for both p and n type materials. In case of the semiconductors like Ge or Si, values of N_C are higher than that of N_V. But the situation is quite different for many of the III-V compound semiconductor materials like GaAs, InP and GaP. In case of these materials, values of N_V are higher than that of N_C. Such variations in relative values of N_C and N_V should be taken into consideration while choosing structures for achieving higher conversion efficiency through higher built in potential [26]. Table 3.1 shows theoretical values of V_D for some heterojunction with both n-on-p and p-on-n structures composed of materials having different values of density of states.

Materials	Band gaps (eV)	Structure	V_D (V)
GaAs/Ge	1.42/0.66	p-on-n	0.43
		n-on-p	0.51
GaAs/Si	1.42/1.12	p-on-n	0.86
		n-on-p	0.96
GaP/Si	2.26/1.12	p-on-n	0.837
		n-on-p	0.864
GaP/InP	2.26/1.34	p-on-n	1.16
		n-on-p	1.08
GaP/GaAs	2.26/1.42	p-on-n	1.24
		n-on-p	1.17

Table 3.1: Built in potentials for different heterostructures with $N_A=N_D=10^{17}$ cm^{-3}. (N_C, N_V) values in per cm^3 for Ge, Si, GaAs, InP and GaP are $(1.04\times10^{19}, 6\times10^{18})$, $(2.8\times10^{19}, 1.04\times10^{19})$, $(4.7\times10^{17}, 7\times10^{18})$, $(5.7\times10^{17}, 1.1\times10^{19})$ and $(1.8\times10^{19}, 1.9\times10^{19})$ respectively.

3.2.3 Open Circuit Voltage

As discussed in chapter 2, the J-V characteristics of any illuminated p-n junction is given by:

$$J = J_L - J_S \left(e^{qV/kT} - 1\right) \tag{3.13}$$

where J_L is photocurrent density and J_S is dark saturation current density. Under open circuit condition no current flows through the external load as all the photonically generated electron-hole pairs recombine within the cell. The open circuit voltage is obtained by putting $J = 0$ in the above equation and is given by

$$V_{OC} = \frac{kT}{q} \ln(1 + \frac{J_L}{J_S})$$

(3.14)

The electron and hole components of dark saturation current, J_{ns} and J_{ps} can be obtained from equation 3.4 and 3.5. Using the expressions for built in potential, given by equations 3.11 and 3.12, the electron and hole components of dark current density for the structure shown in fig. 3.1a becomes

$$J_{ns} = \frac{qD_n}{L_n} N_D e^{-(qV_D - \Delta E_C)/kT} = \frac{qD_n}{L_n} \frac{N_{c1}N_{v2}}{N_A} e^{-E_{g2}/kT}$$

(3.15a)

$$J_{ps} = \frac{qD_p}{L_p} N_A e^{-(qV_D + \Delta E_V)/kT} = \frac{qD_p}{L_p} \frac{N_{c1}N_{v2}}{N_D} e^{-E_{g1}/kT}$$

(3.15b)

In the above expressions, the notch like potential discontinuity ΔE_c, shown in figure 3.1a, has been assumed to be zero.

For the structure shown in Fig.3.2b, these saturation currents are

$$J_{ns} = \frac{qD_n}{L_n} N_D e^{-(qV_D + \Delta E_C)/kT} = \frac{qD_n}{L_n} \frac{N_{c2}N_{v1}}{N_A} e^{-E_{g1}/kT}$$

(3.16a)

$$J_{ps} = \frac{qD_p}{L_p} N_A e^{-(qV_D - \Delta E_V)/kT} = \frac{qD_p}{L_p} \frac{N_{c2}N_{v1}}{N_D} e^{-E_{g2}/kT}$$

(3.16b)

In case of equations 3.16, the notch like potential discontinuity ΔE_v, shown in figure 3.1b, has been assumed to be zero.

Since for both structures E_{g1} is much greater than E_{g2} (see figure 3.1), it is quite clear from the above equations (eq. 3.15-3.16) that in a *p-n* heterojunction structures, either of the electron or hole components of current dominates. In case of fig 3.1a electron current will be dominating where as in fig 3.1b hole current dominates. Using the Einstein

relation in equations 3.15 and 3.16, the influence of mobility of charge carriers on dark saturation current can be visualized:

$$J_{ns} = kT \frac{\mu_n}{L_n} \frac{N_{c1}N_{v2}}{N_A} e^{-E_{g2}/kT} \qquad \text{for fig.3.1a} \qquad (3.17)$$

$$J_{ps} = kT \frac{\mu_p}{L_p} \frac{N_{c2}N_{v1}}{N_D} e^{-E_{g2}/kT} \qquad \text{for fig.3.1b} \qquad (3.18)$$

As the band gap of the high band gap material (E_{g1}) is increased, the dark saturation current becomes almost equal to either J_{ns} (in case of fig 3.1a) or J_{ps} (in case of fig. 3.1b), expressed by equations 3.17 and 3.18. According to equation 3.14, the magnitude of dark saturation current has to be minimized to obtain maximum possible open circuit voltage for a particular short circuit current. In achieving the minimum value of dark saturation current, the product of the mobility and density of state term is the key factor assuming same doping density for both p and n type materials.

3.3 Results and Discussions

A number of p-n heterojunction solar cell structures has been considered to visualize the impact of mobility and density of states on the open circuit voltage (V_{OC}) and efficiency (η). To do so, output power density (P/a) and current density have been plotted as a function of voltage. The output power density has been calculated simply by multiplying current density, given by equation 3.13, with respective voltages:

$$P/a = JV = J_S V (e^{qV/kT} - 1) - J_L V \qquad (3.19)$$

The maximum output power densities have been obtained directly from the power density curves. The conversion efficiency is given by the ratio between maximum power density and input power density. The value of short circuit current density (J_{SC}) has been calculated as a function of band gap of the smaller band gap material (E_{g2} of fig 3.1) from

the curve shown in figure 2.4b of chapter 2. The input power density is also obtained by calculating the area under the above mentioned curve. Air mass 1.5 (AM 1.5) spectrum of the solar radiation has been used for calculating short circuit current and output power density. The values of mobility and diffusion lengths for electrons and holes have been taken from published literatures to produce realistic results [4, 27-29].

The variations of current density and output power density with voltage have been shown in figure 3.2 for various *p*-on-*n* and *n*-on-*p* heterojunctions with different material compositions. The curves shown in dotted lines are for *p*-on-*n* structures and that shown in firm lines are for *n*-on-*p* structures.
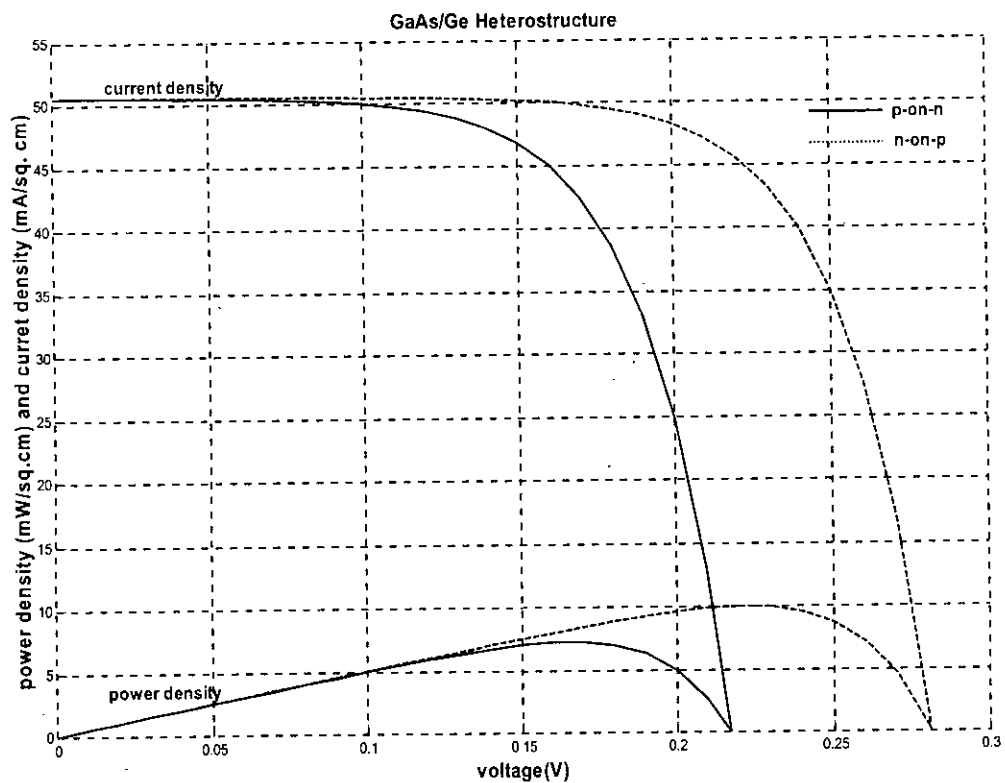

Figure 3.2 a: *J-V* and *P-V* curves for GaAs/Ge heterojunction structures.
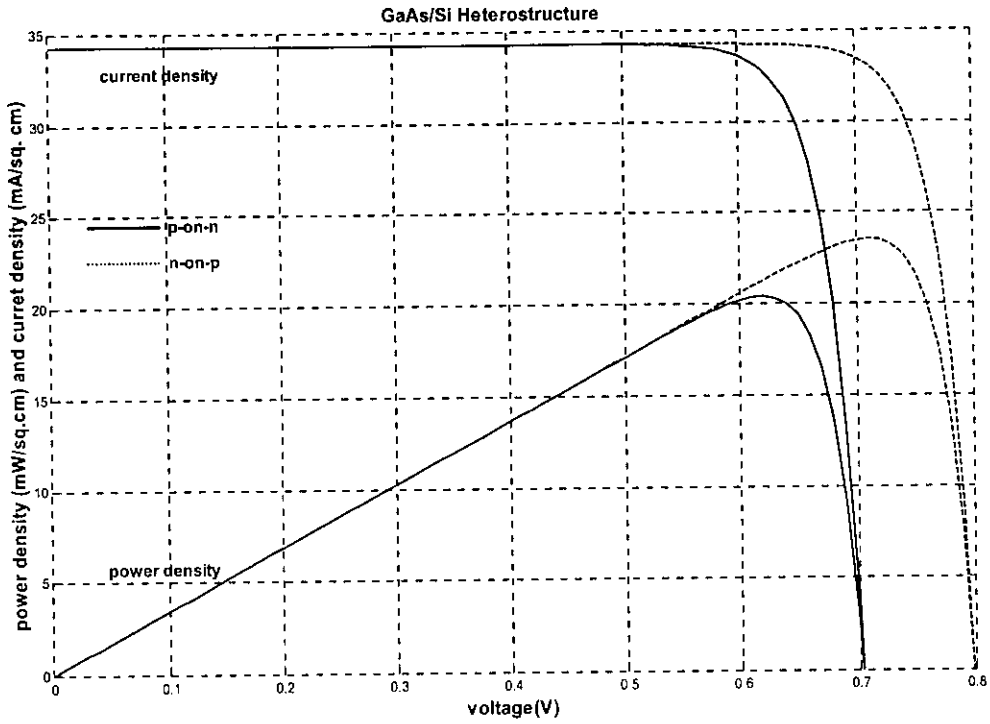
Figure 3.2 b: *J-V* and *P-V* curves for GaAs/Si heterojunction structures.
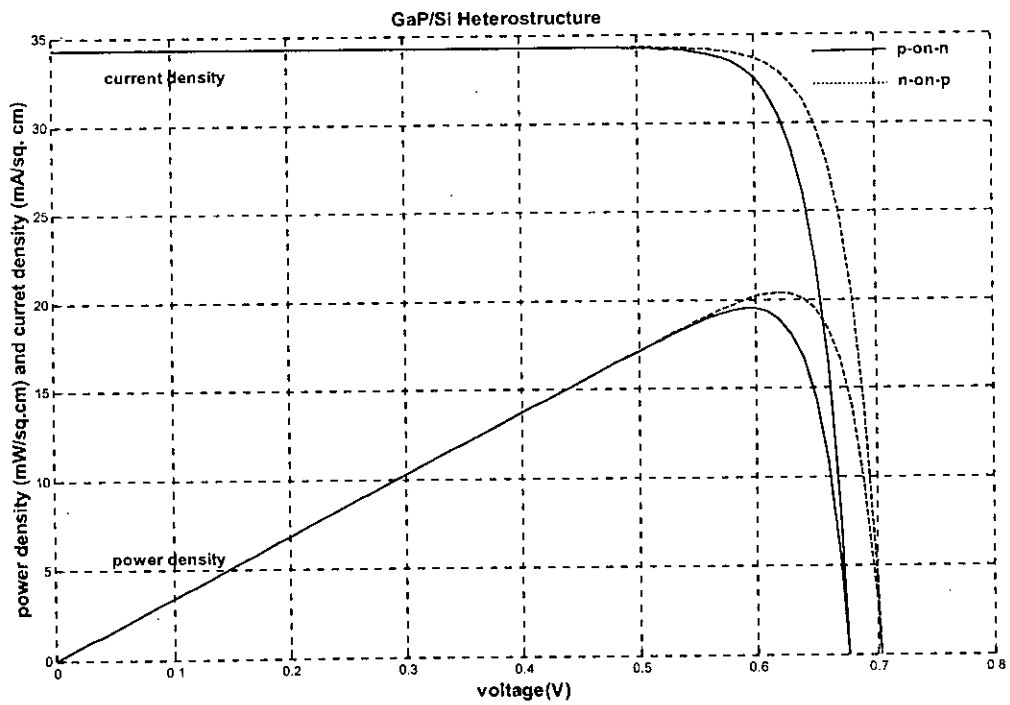
Figure 3.2 c: *J-V* and *P-V* curves for GaP/Si heterojunction structures.
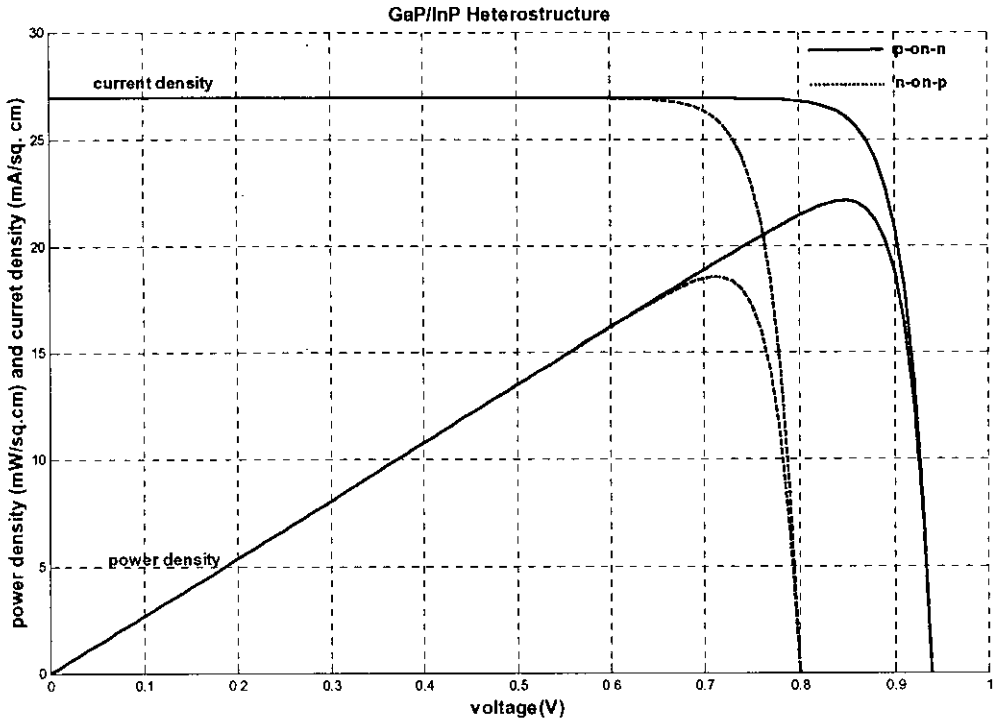
Figure 3.2 d: *J-V* and *P-V* curves for GaP/InP heterojunction structures.
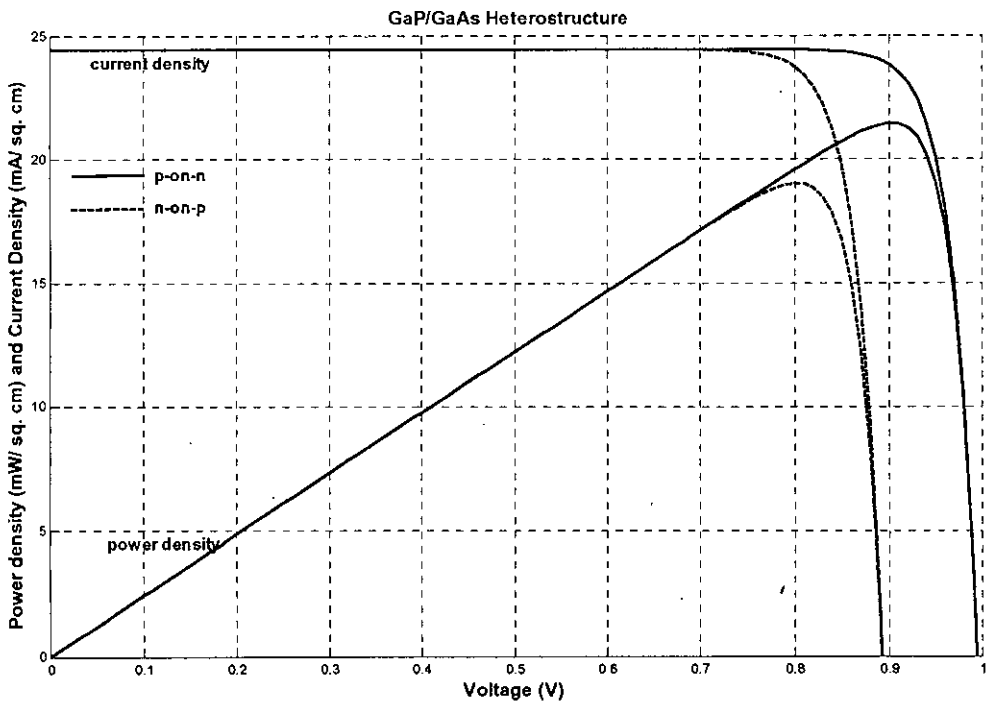
Figure 3.2 e: *J-V* and *P-V* curves for GaP/GaAs heterojunction structures.

For the sake of clear revelation, the calculated values of open circuit voltage (V_{OC}), short circuit current density (J_{SC}), maximum output power density (P_{max}) and conversion efficiency (η) for different p-n heterojunction solar cells have been presented in Table 3.2.

Material	Structure	V_{OC} (V)	J_{SC} (mA/cm^2)	P_{max} (mW/cm^2)	η (%)
GaAs/Ge	p-on-n	0.218	50.58	7.25	8.85
	n-on-p	0.28		10.10	12.33
GaAs/Si	p-on-n	0.7	34.29	20.40	24.99
	n-on-p	0.8		23.52	28.70
GaP/Si	p-on-n	0.678	34.29	19.50	23.80
	n-on-p	0.704		20.40	24.99
Gap/InP	p-on-n	0.94	26.93	22.10	26.97
	n-on-p	0.80		18.5	22.58
GaP/GaAs	p-on-n	0.995	24.46	21.5	26.24
	n-on-p	0.895		19.0	23.19

Table 3.2: Open circuit voltage, maximum power output and efficiency for different heterojunction solar cell structures.

It is interesting to see that open circuit voltage for the same pair of materials in a p-n heterojunction is not the same when p and n type materials are swapped. The short circuit current density, on the other hand, remains unchanged as it has been calculated as a function of E_{g2} (band gap of the lower band gap material) assuming that all photons having energy higher than E_{g2} have contributed one electron. As a result, the conversion efficiency is changed as the n and p type materials are interchanged.

As the mobility of electrons are higher than that of holes, it is expected that p-on-n structures should achieve higher V_{OC} and efficiency than n-on-p structures. But as revealed by the results shown in table 3.2, this is not always true. In fact, open circuit

voltages are higher for *n*-on-*p* structures, if heterojunctions are formed between III-V compound semiconductors and other materials like Ge and Si. The value of N_C is higher than N_V for materials like Ge and Si, but for III-V compound semiconductors (like GaAs, InP, GaP) this is reverse. So, for those *p*-on-*n* structure, the product of N_C and N_V is much higher than that of *n*-on-*p* structures. Even though, the mobility difference between electrons and holes are much higher for *p*-on-*n* structures as compared to *n*-on-*p* structures, the effect is over shadowed for those pair of materials. The dark saturation current, given by equations 3.17 and 3.18, is therefore higher and hence open circuit voltage is lower for *p*-on-*n* structures as compared to that of *n*-on-*p* structures. On the contrary, when heterojunctions are formed between two III-V compound semiconductor materials, open circuit voltage and conversion efficiency is higher for *p*-on-*n* structures as in this case $N_C < N_V$ for both *n*-on-*p* and *p*-on-*n* structures and so the mobility difference between electrons and holes can be exploited more effectively. In case of *p*-on-*n* heterostructures formed with two III-V compound semiconductors, dark current is entirely dominated by holes and so it becomes much lower than that of *n*-on-*p* structures where it is dominated by electrons. These facts become conspicuous from table 3.2, which shows that much higher open circuit voltage and efficiency can be achieved if *p*-on-*n* structure is used instead of *n*-on-*p* structures formed between two III-V compound semiconductor materials.

3.4. Conclusions

The influence of some parameters like density of states and mobility in determining conversion efficiency have been high lighted and based on that some suggestions have been made for exploiting theses parameters in making high efficiency heterojunction solar cells. The results of this chapter show that the open circuit voltage and hence conversion efficiency for a *p*-*n* heterojunction solar cell is not same if the *p* and *n* type materials are interchanged. Generally speaking, the value of N_V is higher than that of N_C and the mobility difference between electrons and holes are much prominent for III-V compound semiconductor materials. When *p*-*n* heterojunction solar cell is made from

such materials, the band gap of the p-type material must be higher than that of n- type material to reduce dark saturation current and hence to achieve higher open circuit voltage and conversion efficiency. It is noteworthy that the efficiency of a p-GaP/n-GaAs heterojunction solar cell is higher than that of p-GaAs/n-GaP cell by more than 13%. Even better improvement, around 19%, can be achieved if p-GaP/n-InP heterostructure are used instead of p-InP/n-GaP heterostructure as solar cells.

CHAPTER 4

HETEROFACE SOLAR CELLS

4.1 Introduction

There are mainly two reasons behind low conversion efficiency of a single material *p-n* junction solar cell. First, as *p-n* junction responds only to the photons with quantum energy higher than the band gap of its material, a single material homojunction solar cell fails to absorb all the photons within incoming solar radiation. The photons with energy less than the band gap of the material are not absorbed at all and are lost. The second reason is the loss introduced by the internal recombination of the photogenerated carriers within the cell. Under illuminating condition, a *p-n* junction becomes forward biased due to the accumulation of electrons and holes in *n*-type and *p*-type materials respectively. Due to such forward biasing, the potential barrier of the junction is reduced and a portion of the photogenerated charge carriers overcome the barrier and ultimately recombine within the cell. This leaves fewer charge carriers available to flow through the external load. It was pointed out in the earlier chapters that although photons with wider range or band of energies can be absorbed by using materials with low energy gap, use of such low band gap materials would increase the rate of internal recombination of photogenerated carriers. In case of junctions formed by materials with low energy gap, the built in potential becomes much smaller which causes easy flow of photogenerated carriers over the junction. It has been reported that the optimum band gap for such single material *p-n* junction solar cell, under the concentration of 1 sun, is 1.35 eV [23] which is close to the band gaps of InP and GaAs.

To alleviate the above mentioned limitations, heteroface solar cells were proposed where a layer of high band gap material has been added to a typical *p-n* homojunction. The *p-n* homojunction layer is used to absorb the low energy photons of solar radiation. The high band gap layer is, on the other hand, used to minimize the internal recombination by

offering higher potential barrier to either electrons or holes generated by optical excitation. The high band gap material also helps to enhance spectral response of the cell by absorbing high-energy photons more efficiently just like a heterojunction solar cell. A heteroface solar cell with a GaAs *p-n* homojunction and an added layer of high band gap *p*-type $Al_xGa_{1-x}As$, was introduced in 1973 [11]. The conversion efficiency of this cell, having *p*-$Ga_{1-x}Al_xAs$/*p*-GaAs/*n*-GaAs structure, has been reported to be more than 22% [11-12]. The efficiency of such heteroface solar cells are limited by the fact that it is not possible to use arbitrary small band gap material to fabricate the *p-n* junction as that would increase the rate of internal recombination of either of the carriers whose flow is not prevented by the layer of high band gap material.

In this chapter the analytical expressions for a heteroface solar cell have been developed first to predict their theoretical conversion efficiency. Then it have been shown that even better conversion efficiency can be achieved if, instead of a *p-n* homojunction layer, a *p-n* heterojunction layer is used with the layer of high band gap material. Because in case of the later structure with heterojunction layer, it would be possible to create reasonably high potential barrier for both electrons and holes. At the same time it would be possible to absorb even wider band of the solar radiation spectrum by using the low band gap material of the heterojunction.

4.2 Analysis of Heteroface Solar Cells

A heteroface solar cell has been analyzed analytically in this section. Figure 4.1 shows the band diagram of a heteroface structure having a *p-n* homojunction layer with a high band gap *p*-type material. The band gap of the material forming *p-n* homojunction layer
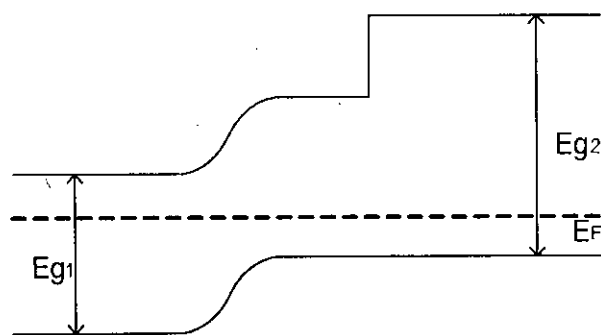
Figure 4.1: Energy band diagram of a heteroface cell under equilibrium condition.

is E_{g1} and the band gap of added p-type material is E_{g2} where $E_{g2}>E_{g1}$. Light usually enters through the high band gap layer which is therefore termed as window layer. The photons with quantum energy less than E_{g2} passes through the window layer and are ultimately absorbed in the p-n homojunction layer. In case of the structure shown in figure 4.1, the transition to the window layer is abrupt. Also Heteroface structures with graded gap window layer adjacent to the p-n homojunction layer have been reported [9]. In both cases, it has been assumed that the high band gap p-type material works as a window to the incoming photons having energy less than E_{g2}. But as pointed out in this thesis, the main purpose of this layer is to increase the potential barrier to photogenerated electrons and hence minimize the dark saturation current.
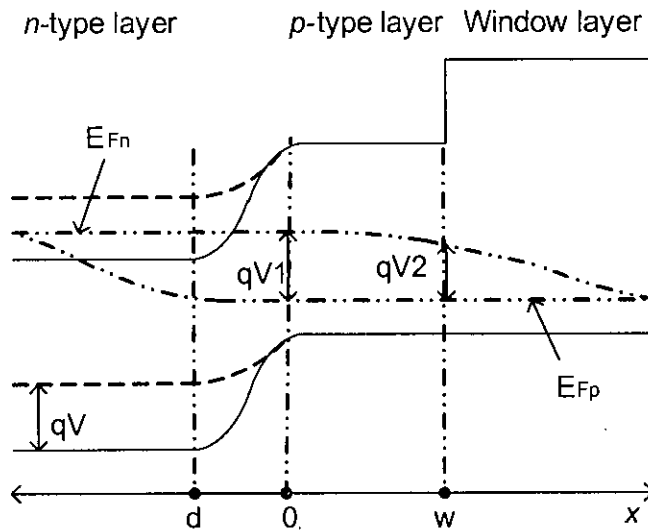
Figure 4.2: Energy band diagram of a heteroface solar cell under illumination.

When illuminated, photons are mainly absorbed in the p-n homojunction layer and so, as discussed in chapter 2, the junction becomes forward biased. Figure 4.2 shows the energy band diagram of the structure under illuminating condition. As the p-n junction becomes forward biased, the potential barrier is reduced and the Fermi levels for electrons and holes are separated. The quasi Fermi levels for both electrons and holes have been assumed to be flat across the depletion region of p-n junction according to the quasi-Fermi level assumption [9]. The separation between the quasi Fermi levels for electrons and holes at $x = 0$, gives the voltage developed across the depletion layer of p-n

homojunction (V_I) and the total voltage developed across the cell (V) as well. The quasi Fermi level E_{Fn} for electrons has been shown to decrease slightly to allow recombination of electrons in the p-type material of the p-n homojunction. On the other hand, the quasi Fermi level for holes has been assumed to be same in both p-type materials implying same work function for the materials. The total voltage, V is given by the difference between the quasi Fermi levels for electrons in the n-type material and for holes in the p-type material forming the window layer. The voltage developed across the abrupt junction between the p-type material of p-n homojunction and the window layer has been represented by V_2 and is given by the difference between the quasi Fermi levels for electrons and that of holes at $x = w$. Due to recombination of electrons in the p-type layer, V_2 is slightly less than V or V_I.

As mentioned earlier, the potential barrier of the p-n junction is reduced due to illumination and so more electrons become successful to overcome this barrier. Some of these electrons recombine in the p-type layer causing the quasi Fermi level for electrons to drop slightly. It is clearly seen from figure 4.2 that the ultimate barrier for electrons is much higher than that of holes. To get an analytical expression for the electron and hole components of the current (termed as dark current in chapter 2), we have to find the expressions for minority carrier distributions in n-type, p-type and window layers first.

For a neutral region of a semiconductor where no electric field is present, the distribution of excess electrons, assuming low injection, is given by the following partial differential equation:

$$\frac{\partial^2 \Delta n(x)}{\partial x^2} - \frac{\Delta n(x)}{D_n \tau_n} = 0 \qquad (4.1)$$

where $n(x)$ is excess electron concentration at any point x and D_n, τ_n are diffusion constants and life times for electrons in the neutral region.

We will first find the excess electron density distribution in the p-type layer ($0 \le x \le w$) and in the window layer ($x \le w$), as shown in figure 4.2. This electron distribution can be found by solving equation 4.1. The excess electron density in base region ($0 \le x \le w$) can be expressed as

$$\Delta n_p(x) = C_1 e^{-x/L_{np}} + C_2 e^{x/L_{np}} \tag{4.2}$$

For window layer, on the other hand, the distribution is given by:

$$\Delta n_w(x) = C_3 e^{-(x-w)/L_{nw}} \tag{4.3}$$

where C_1, C_2, C_3 are arbitrary constants and $L_{np,nw}$ are diffusion lengths of electrons in p-type and window layers respectively. The boundary conditions for the heteroface structure under consideration are the followings:

$$\text{at } x = 0, \; C_1 + C_2 = n_{pop}(e^{qV_1/kT} - 1) = \Delta n_o \tag{4.4a}$$

$$\text{at } x = w^-, \; C_1 e^{-w/L_{np}} + C_2 e^{w/L_{np}} = n_{pop}(e^{qV_2/kT} - 1) = \Delta n_w \tag{4.4b}$$

$$\text{at } x = w^+, \; C_3 = n_{pow}(e^{qV_2/kT} - 1) \tag{4.4c}$$

where Δn_o and Δn_w represent the excess electron concentration at $x = 0$ and $x = w$ respectively. Here n_{pop} and n_{pow} represent the equilibrium electron concentration in the p-type and window layer respectively. These minority carrier concentrations exponentially decrease with the band gaps of the respective layers. n_{po} can be expressed in terms of band gap by the following equation [4]:

39

$$n_{po} = n_i^2/N_A = \frac{N_C N_V e^{-E_g/kT}}{N_A}$$

Similarly, equilibrium hole concentration in any *n*-type material can be expressed as:

$$p_{no} = n_i^2/N_D = \frac{N_C N_V e^{-E_g/kT}}{N_D}$$

where n_i is the intrinsic carrier concentration. The electron current density in the window layer as a function of x can be given by

$$J_{nw}(x) = \frac{qD_{nw}}{L_{nw}}\frac{\partial \Delta n_w(x)}{\partial x} \quad (\text{for } x > w) \tag{4.5a}$$

Using equation 4.3 and 4.4c, the electron current density at $x=w^+$,

$$J_{nw} = -\frac{qD_{nw}}{L_{nw}} n_{pow}(e^{qV_2/kT} - 1) \tag{4.5b}$$

Similarly electron current density as a function of x in the *p*-type region is given by

$$J_{np}(x) = \frac{qD_{np}}{L_{np}}\frac{\partial \Delta n_p(x)}{\partial x} \tag{4.6}$$

The values of C_1 and C_2 can be found by solving boundary conditions 4.4a and 4.4b:

$$C_1 = \frac{\Delta n_o e^{w/L_{np}} - \Delta n_w}{e^{w/L_{np}} - e^{-w/L_{np}}}, \quad C_2 = \frac{\Delta n_w - \Delta n_0 e^{-w/L_{np}}}{e^{w/L_{np}} - e^{-w/L_{np}}} \tag{4.7}$$

It is interesting to note that for w , $C_1 = n_{pob}(e^{qV_1/kT} - 1)$ and $C_2 = 0$. So the excess electron distribution in the p-type material becomes

$$\Delta n_p(x) = n_{pop}(e^{qV_1/kT} - 1)e^{-x/L_{np}}$$

which is identical to a p-n homojunction. It is also quite visible from equation 4.4c that, since equilibrium minority carrier concentration (n_{po}) decreases exponentially with energy band gap of the material, C_3 and hence n_w approaches zero as the band gap of the window layer (E_{g2}) approaches infinity. This is quite reasonable because if such high band gap window layer is used, almost no electron will be able to surmount the abrupt barrier at the transition from the p-type layer to the window layer.

Combining equation 4.6 ad 4.7 we get the expressions for electron current density at $x = w^-$,

$$J_{np}(x = w^-) = \frac{qD_{np}}{L_{np}} \frac{n_{pop}(e^{qV_2/kT} - 1)(e^{w/L_{np}} - e^{-w/L_{np}}) - 2n_{pop}(e^{qV_1/kT} - 1)}{e^{w/L_{np}} - e^{-w/L_{np}}}$$

(4.8a)

Assuming both qV_1 and qV_2 much higher than kT and $w/L_{np} \ll 1$,

$$J_{np}(x = w^-) = \frac{qD_{np}}{L_{np}} n_{pop} \frac{L_{np}}{w}(e^{qV_2/kT} - e^{qV_1/kT})$$

(4.8b)

According to current continuity condition, J_{np} (at $x = w^-$) $= J_{nw}$ (at $x = w^+$). Putting the values of corresponding current densities from equation 4.8 and 4.5b, we get

$$-\frac{qD_{nw}}{L_{nw}}n_{pow}e^{qV_2/kT} = \frac{qD_{np}}{L_{np}}n_{pop}\frac{L_{np}}{w}(e^{qV_2/kT} - e^{qV_1/kT}) \qquad (4.9a)$$

or,

$$e^{qV_1/kT} = (1 + \frac{n_{pow}D_{nw}w}{n_{pop}D_{np}L_{np}})e^{qV_2/kT} \qquad (4.9b)$$

Since E_{g2} is reasonably higher than E_{g1} and equilibrium minority carrier concentration decreases exponentially with band gap, it is quite obvious that $n_{pow} \ll n_{pop}$. Moreover it has been assumed that $w \ll L_{nw}$. Also the mobility and hence diffusion constants decreases considerably in case of high band gap materials (for example $Al_xGa_{1-x}As$, GaP etc.). So it can be safely assumed that $D_{nw} < D_{np}$ and hence the second term within the bracket in the right hand side of the above equation can be ignored in comparison to 1. Then for all practical condition,

$$V_1 \approx V_2 \approx V \qquad (4.10)$$

It implies that by making the p-type layer very thin compared to the diffusion length of electrons in that layer (i.e. $w/L_{np} \ll 1$), it is possible to minimize the recombination of electrons to such an extent that the quasi Fermi level for electrons remains practically flat across the p-type material.

Due to the above condition Δn_0 becomes almost equal to Δn_w and the expressions for C_1 and C_2 are slightly modified,

$$C_1 = \Delta n_0 \frac{1 - e^{-w/L_{nb}}}{1 - e^{-2w/L_{nb}}}, C_2 = \Delta n_0 \frac{e^{-w/L_{nb}} - e^{-2w/L_{nb}}}{1 - e^{-2w/L_{nb}}} \qquad (4.11)$$

The electrons from the n-type layer, successful to overcome the potential barrier of the p-n junction, either recombines with the holes within the p-type layer or enter the window layer. So the total electron current density at $x = 0$ can be shown as summation of two components.

$$J_n \text{ (at } x = 0) = J_{npr} + J_{nw} \text{ } (at \text{ } x = w^+)$$

(4.12)

The first component (J_{npr}), which depends exponentially on the voltage V_1, is given by the recombination rate of the electrons within the base layer. The second component (J_{nw}), which exponentially depends on the voltage V_2, is given by the rate at which electrons become successful to surmount the abrupt barrier between the p-type and window layer. The recombination current, J_{npr} can be expressed by

$$J_{npr} = -q \frac{\Delta N}{\tau_{np}}$$

(4.13)

where ΔN is the total number of excess electrons in the base region and is given by

$$\Delta N = \int_0^w \Delta n_p(x)dx$$

(4.14a)

Using equation 4.2, 4.10, 4.11 and 4.12, the final expression for ΔN becomes

$$\Delta N = 2n_{pop}L_{np} \frac{1 - e^{-w/L_{np}}}{1 + e^{-w/L_{np}}} (e^{qV/kT} - 1)$$

(4.14b)

Putting this value of ΔN and using the fact that $L_{np} = (D_{np}\tau_{np})$, we get the final expression for J_{npr}:

$$J_{npr} = -2q\frac{D_{np}}{L_{np}}n_{pop}\frac{1-e^{-w/L_{np}}}{1+e^{-w/L_{np}}}(e^{qV/kT}-1) \qquad (4.15a)$$

$$= -2q\frac{D_{np}}{L_{np}}n_{pop}\frac{w/L_{np}}{2-w/L_{np}}(e^{qV/kT}-1) \quad \text{(assuming } w/L_{np} \ll 1) \quad (4.15b)$$

Finally, according to equation 4.12, the expression for electron current density at $x = 0$ can be obtained by using equation 4.5b and 4.15 as:

$$J_n \text{ (at } x = 0) = -q(2\frac{D_{np}}{L_{np}}n_{pop}\frac{w/L_{np}}{2-w/L_{np}}+\frac{D_{nw}}{L_{nw}}n_{pow})(e^{qV/kT}-1) \qquad (4.16a)$$

$$= J_{ns}(e^{qV/kT}-1) \qquad (4.16b)$$

where J_{ns} represents the voltage independent part of the above equation and termed as dark saturation current.

The hole component of dark current (J_p) density for the heteroface structure can be easily found by normal Shockley equations [4]. This is because for holes the only barrier existing is the junction potential barrier between top and base layer. So the expression for hole component of dark current density can be expressed as

$$J_p \text{ (at } x = 0) = q\frac{D_{pn}}{L_{pn}}p_{no}(e^{qV/kT}-1) \qquad (4.17a)$$

$$= J_{ps}(e^{qV/kT}-1) \qquad (4.17b)$$

44

where D_{pn} and L_{pn} represents diffusion coefficient and diffusion length of holes and P_{no} represents the equilibrium hole concentration in n-type layer. Here also, J_{ps} represents the saturation current. The total dark current density at $x = 0$, is of course given by the summation of the electron and hole current components given by equation 4.16 and 4.17.

As explained in chapter 2, under open circuit condition all the photogenerated carriers ultimately recombine internally and so the total dark current becomes exactly equal to the short circuit current. So the open circuit voltage V_{OC} can be calculated as usual by equating dark current density to the short circuit current density (J_{SC}):

$$V_{OC} = \frac{kT}{q} \log(1 + \frac{J_{SC}}{J_{ns} + J_{ps}}) \tag{4.18}$$

According to equations 4.16 and 4.17, both J_{ns} and J_{ps} depends on the band gaps of n-type and window layers respectively, through the minority carrier concentrations (n_{pow} and p_{no}) in the mentioned layers. So, as seen from equation 4.18, the open circuit voltage is expected to increase if the band gaps of those layers are increased.

4.3 Analysis of the Structures having a p-n Heterojunction with a Window Layer

In case of heteroface structures discussed in the previous section, a window layer has been used to reduce the electron component of the dark saturation current by creating higher potential barriers for electrons. In fact it has been shown in the next section that as the band gap of window layer is increased, the electron component of dark saturation current becomes negligible as compared to that of hole component. So it is quite obvious that the open circuit voltage can be increase further by creating higher potential barrier for holes also. If this can be done without reducing the short circuit current, considerable improvement in conversion efficiency can be achieved. This section proposes a structure, which provides such a higher potential barrier for holes by using a p-n heterojunction, instead of p-n homojunction, with a window layer. With this structure, it is possible to

reduce both electron and hole component of dark saturation current with out any reduction of short circuit current. In fact use of p-n heterojunction will improve the photo response as two different band gap material cam be exploited to absorb a wider band of solar radiation more efficiently.
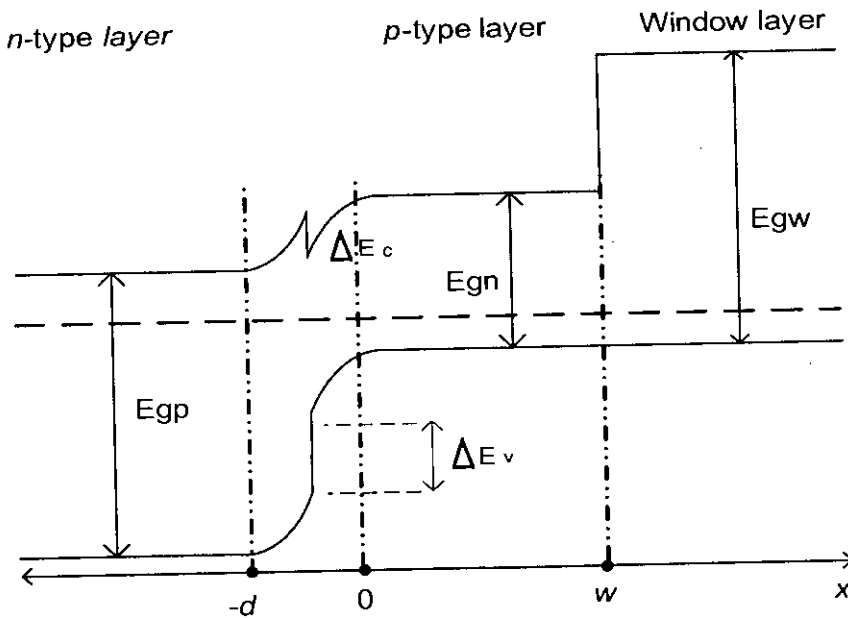
Figure 4.3: A Solar cell structure with heterojunction and window layer under equilibrium condition.

Figure 4.3 shows a solar cell structure consisting of a heterojunction of a wide band gap n-type material and narrow band gap p-type material along with a high ban gap p-type window layer. It is quite obvious that, with this structure, it would be possible to suppress both the electron and hole components of dark current. At the same time, it would be possible to absorb the photons of a much wider band of solar radiation by the low band gap p-type material of the heterojunction.

The analysis of this structure can be carried out exactly in the similar fashion as we did in the previous section for the heteroface structure. The notch like discontinuity between the conduction bands of n-type and p-type layer has been ignored. So the expressions derived for the heteroface structure remains unchanged for this structure. However, as two different band gap n and p type materials are used to form heterojunction, different values

of density of states corresponding to the materials have to be used in calculating the equilibrium minority carrier concentrations (p_{no} and n_{po}) in p-type and n-type materials respectively.

The expressions for equilibrium minority carrier density at n-type, p-type and window layers can be expressed in terms of density of states and band gaps of the corresponding materials:

$$p_{no} = \frac{n_{in}^2}{N_{An}} = \frac{N_{Cn}N_{Vn}}{N_{An}} e^{-E_{gn}/kT} \tag{4.19a}$$

$$n_{pop} = \frac{n_{ip}^2}{N_{Dp}} = \frac{N_{Cp}N_{Vp}}{N_{Dp}} e^{-E_{gp}/kT} \tag{4.19b}$$

$$n_{pow} = \frac{n_{iw}^2}{N_{Dw}} = \frac{N_{Cw}N_{Vw}}{N_{Dw}} e^{-E_{gw}/kT} \tag{4.19c}$$

where $n_{in,p,w}$ represents intrinsic carrier concentrations and $N_{An,Dp,Dw}$ represents doping density in n-type, p-type and window layers respectively.

The final expressions for dark current density and open circuit voltage can be obtained by putting these values of equation 4.19 into equations 4.16, 4.17 and 4.18. So the dark current density for the structure presented in this section is given by:

$$J_s = q\left(2\frac{D_{np}}{L_{np}}\frac{N_{Cp}N_{Vp}}{N_{Dp}}e^{-E_{gp}/kT}\frac{w/L_{np}}{2-w/L_{np}} + \frac{D_{nw}}{L_{nw}}\frac{N_{Cw}N_{Vw}}{N_{Dw}}e^{-E_{gw}/kT} + \frac{D_{pn}}{L_{pn}}\frac{N_{Cn}N_{Vn}}{N_{An}}e^{-E_{gn}/kT}\right) \tag{4.20}$$

In the above equation, summation of first two terms represents electron component and third term represents hole component of dark saturation current.

4.4 Results and Discussions

4.4.1 Heteroface Structures:

A heteroface solar cell with n-GaAs/p-GaAs/p-Al$_x$Ga$_{1-x}$As structure was studied analytically to highlight the importance of various factors in determining open circuit voltage, short circuit current and hence the efficiency. The short circuit current has been calculated from figure 2.4b of chapter 2 [7], assuming that all photons having energy higher than E_{g1} (fig 4.1) will contribute one electron. The total dark saturation current for this structure can be expressed as

$$J_s = (2q \frac{D_{np}}{L_{np}} n_{pop} \frac{w/L_{np}}{2 - w/L_{np}} + q \frac{D_{nw}}{L_{nw}} n_{pow}) + q \frac{D_{pn}}{L_{pn}} p_{no} \tag{4.21}$$

As mentioned earlier, since n_{pon}, n_{pow} and p_{no} decrease exponentially with their corresponding band gaps, the dark current density and also the open circuit voltage depends on the respective band gaps. In figure 4.4, the calculated value of open circuit voltage has been presented as a function of the band gap of the window layer. It is observed that open circuit voltage increases exponentially with the window layer band gap up to a certain value and then becomes saturated. This is because, when the band gap of window layer approaches to a high value almost no electron succeeds to overcome the abrupt barrier between base and window layer. So, the second component of electron current, expressed by equation 4.16a, becomes negligible as compared to the other components of currents. Also, as w is much smaller than L_{np}, the first term within the bracket representing the electron current due to recombination is also very small. As a result for high values of E_{gw}, dark current is almost entirely carried out by the holes and so open circuit voltage becomes constant with respect to the band gap of the window layer.

Open circuit voltage as a function of the band gap of window layer
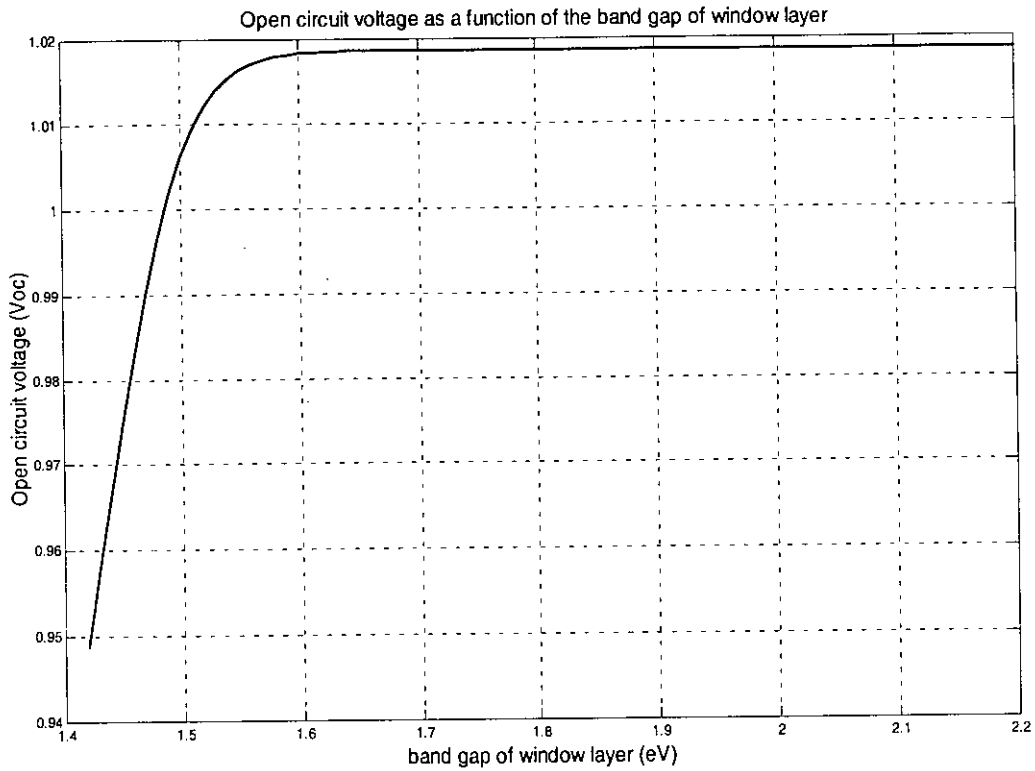
Figure 4.4: Open circuit voltage as a function of the band gap of window layer.

In figure 4.5, the *J-V* characteristics and the variation of power density with load voltage has been presented. In calculating the results the mobility values have been chosen in accordance with the published result [27-29]. The doping density in both *n*-type and *p*-type layer have been assumed to be 10^{17} cm^{-3}. The results have been shown for three different band gaps (E_g of fig. 4.1): 1.34, 1.42 and 1.5 eV of *n* and *p* type layers. The first two band gaps correspond to InP and GaAs respectively. For the third one, material parameters corresponding to GaAs have been used. The band gap of the *p*-type Al$_x$Ga$_{1-x}$As window layer has been assumed to be 1.99eV. It is seen from the figure that short circuit current decreases and open circuit voltage increase with the band gaps of *p* and *n* layers. It is interesting to note that J_{SC} and V_{OC} increase for decrement and increment of the *n-p* homojunction layer band gap from 1.42 eV, corresponding to the band gap of GaAs. But in both cases the maximum out put power density decreases.

49
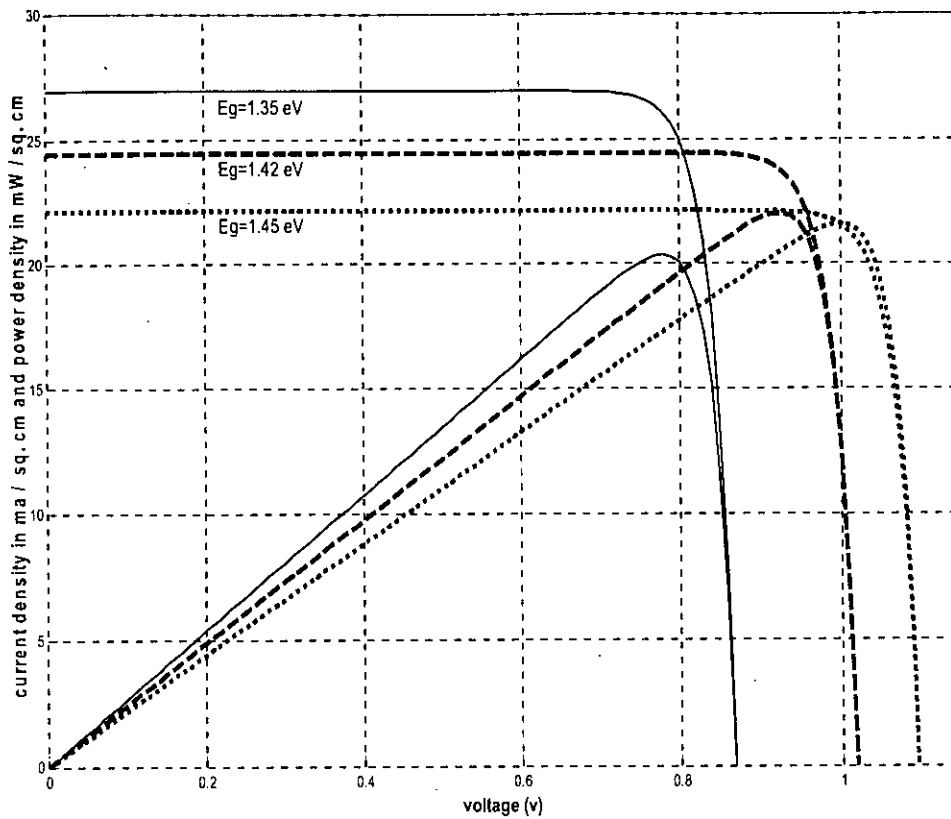
Figure 4.5: Current and power density as a function of voltage for different band gaps of
n and *p* layer.

4.4.2 Solar Cell Structures Composed of Heterojunction and Window Layer

This section presents the results obtained by using the expressions developed in section
4.2 and 4.3 for the structure with heterojunction and window layer. A *n*-GaAs/*p*-Si/*p*-
$Al_xGa_{1-x}As$ structure have been studied and the results have been compared with typical
heteroface and other structures proposed for solar cell.

As can be seen from equation 4.20 and 4.18, the dark saturation current and hence open
circuit voltage depends on the band gap of *n*, *p* and window layers. The open circuit

50

voltage will increase if the band gaps of any of the three layers is increased. But, since the low band gap p layer absorbs the low energy photons, increasing the band gap of this layer can be detrimental as far as short circuit current is concerned. Figure 4.6 represents the variation of open circuit voltage as a function of the band gaps of n-type and window layers .It is seen from figure 4.6 that, like the heteroface structure, here also V_{OC} becomes saturated as either E_{gn} or E_{gw} approaches higher value.
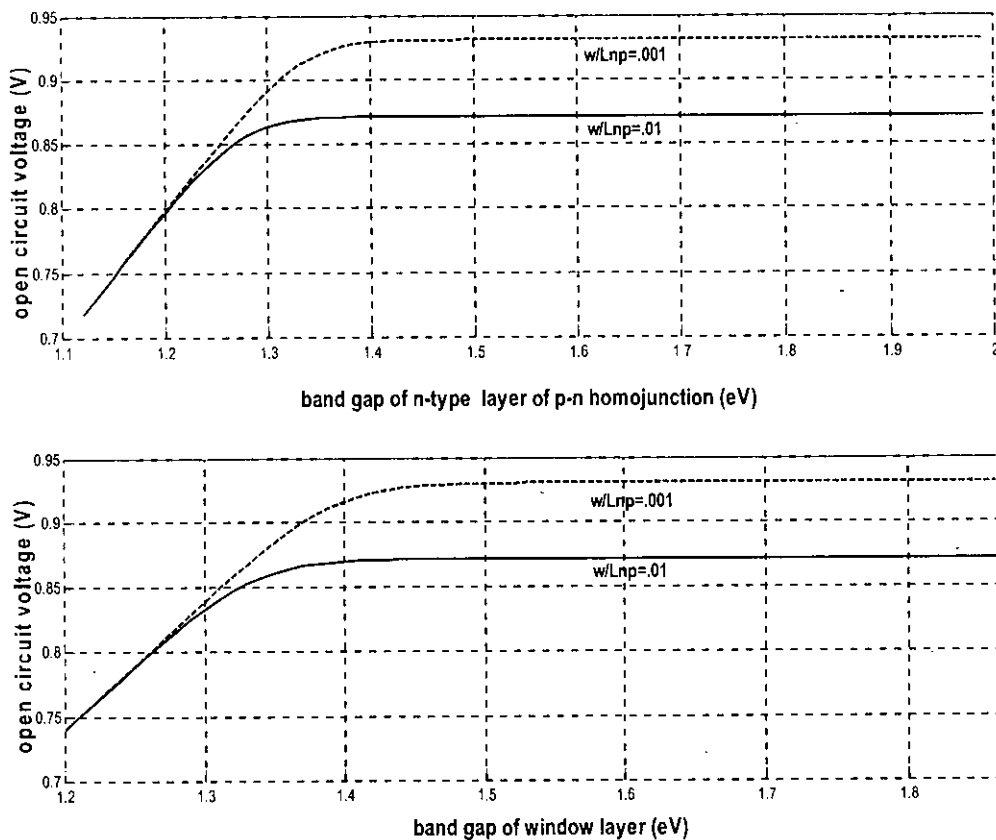
Figure 4. 6: Variation of V_{OC} with the band gaps of n-type and window layer

When E_{gn} approaches higher value dark current is entirely carried by electrons. On the other hand, when E_{gw} is increased hole component of dark current becomes dominant. Figure 4.6 also reveals the effect of p-layer width on open circuit voltage. As the width is decreased, the component of dark current due to the recombination of electrons in the p-

51

layer becomes smaller. So it is quite expected that open circuit voltage increases in both cases as w/L_{np} decreases.

The current density and power density variation with load voltage for n-GaAs/p-Si/p-Al$_x$Ga$_{1-x}$As structure has been presented in figure 4.7. The figure also shows the variation of the characteristics with the band gap of p-layer of the p-n heterojunction. It is revealed from figure 4.7 that the short circuit current can be improved by choosing low band gap material for p-layer.
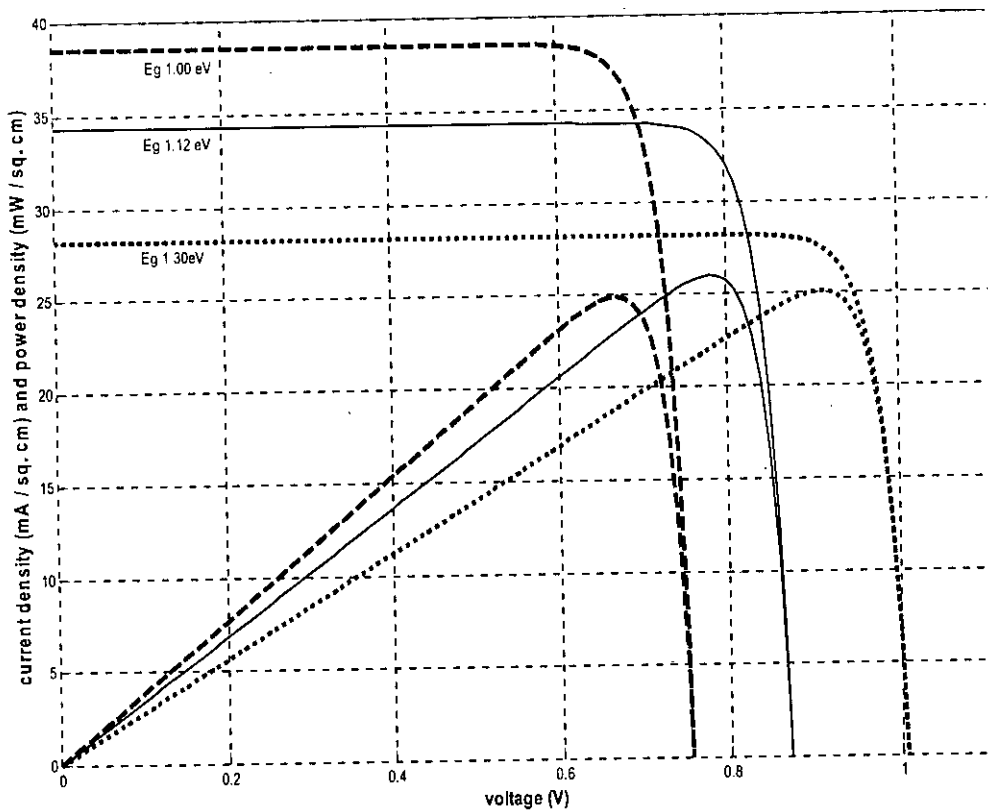
Figure 4.7: *J-V* and *P-V* characteristics of n-GaAs/p-Si/p-Al$_x$Ga$_{1-x}$As.

But at the same time the open circuit voltage reduces with such choice. So Power density although first increases with the decrease of the energy gap of p-layer, it ultimately reaches a maximum value and then start to decrease with further reduction of the band gap of p-layer.

Structure	J_{SC} (mA/cm^2)	V_{OC} (V)	P_{max} (mW/cm^2)	η %
p-n homojunction of GaAs	24.46	0.981	21.10	25.75
n-GaAs/*p*-GaAs/*p*-AlGaAs	24.46	1.019	22.00	26.84
n-AlGaAs/*n*-GaAs/*p*-GaAs/*p*-AlGaAs	24.46	1.100	23.94	29.22
n-GaAs/*p*-Si/*p*-AlGaAs	34.30	0.872	25.95	31.67

Table 4.1: short circuit current, open circuit voltage, maximum output power density and efficiency for various solar cell structures.

Finally table 4.1 shows some comparative results among *p-n* homojunction of GaAs, *n*-GaAs/ *p*-GaAs/ *p*-Al$_x$Ga$_{1-x}$As (heteroface), *n*-GaAs/*p*-Si/*p*-Al$_x$Ga$_{1-x}$As (heterojunction with window layer) and *n*-Al$_x$Ga$_{1-x}$As / *n*-GaAs/ *p*-GaAs/ *p*- Al$_x$Ga$_{1-x}$As. In case of the last structure the hole component of dark current also has the form similar to the electron component of dark current given by equation 4.16. The last structure with double window layer shows better performance than conventional heteroface structure. This is because, in case of the last structure, both electron and hole components of dark current have been reduced by window layers on both sides of the cell. It is clearly visible from table 4.1 that conversion efficiency can be improved by both the new structures proposed by this thesis and it is maximum for *n*-GaAs/*p*-Si/*p*-Al$_x$Ga$_{1-x}$As (heterojunction with window layer) structure.

4.5 Conclusions

This chapter has revealed that heteroface structures can achieve higher conversion efficiency than typical *p-n* homojunction solar cells by suppressing one of the components of dark current. The efficiency can be improved even further, as shown in table 4.1, if two window layers are used with a *p-n* homojunction. But both these structures face the same limitation as single homojunction solar cells regarding photo response. To avoid this limitation, a structure composed of a *p-n* heterojunction and a *p*-

type window layer has been proposed. In this structure, photons with wider band of energies can be absorbed using materials of different band gaps forming the heterojunction and at the same time higher open circuit voltage can be achieved by reducing both electron and hole components of dark current. The calculated results show that the efficiency of this proposed structure is 22% and 17% higher, as compared to *p-n* homojunction and heteroface structures respectively.

CHAPTER 5

CONCLUSIONS

5.1 Discussions

In this thesis the reasons behind the low conversion efficiency of a *p-n* homojunction solar cells has been studied and some heterojunction structures and strategies have been proposed to improve the scenario. This work has pointed out that the mobility difference between electrons and holes along with the variation in density of states for different materials forming heterojunction can be exploited to improve the conversion efficiency. The conversion efficiency of *p-n* heterojunction solar cells depends on the orientation of *p* and *n* type materials and so in some cases the efficiency can be improved significantly by just rearranging the *p* and *n* type materials of the heterojunction structure. This work has also proposed a structure for solar cell where a *p-n* heterojunction has been used along with a high band gap material to increase the overall efficiency. This structure, which is a modification of heteroface solar cell [11-12], has shown considerable promise in achieving higher conversion efficiency.

5.1.1 Rearranging *p* and *n* Type Materials of a *p-n* Heterojunction Structure

A *p-n* junction subjected to shinning becomes forward biased and its potential barrier is reduced. Consequently, a considerable portion of photogenerated carriers is lost through the internal recombination of the carriers successful to overcome that reduced potential barrier. This gives rise to the dark current which depends on electron and hole mobility in the cell material for a particular doping density and voltage. The reported works mainly concentrated on the band gap of the *p-n* junction structures without giving due consideration to the fact that this difference between the mobility of the electrons and

holes can play an important role in determining the overall efficiency of a solar cell [26]. This work has pointed out that, since the potential barriers for electrons and holes are not equal in a p-n heterojunction, such mobility difference of electrons and holes can be exploited effectively for achieving higher conversion efficiency using such structure. As the mobility of electrons are much higher than the mobility of hole, the structures having higher potential barrier for electrons (known as p on n structure) is expected to have higher efficiency than the structures having higher barrier for holes (known as n on p structure). But it has been shown in chapter 3 that, the built in potential barrier, which is another determining factor of the magnitude of dark current density, is not same for the two above mentioned heterojunction structures if same doping density is used for both p and n type materials. It is seen from the expressions presented, that built in potential depends on the density of states in conduction and valence bands (N_C and N_V respectively) of n and p type materials of the heterojunction. So the conversion efficiency does not remain same if n and p type materials are interchanged. In fact, the dark current density depends on the product of respective carrier mobility and density of sates in valence and conduction bands. For semiconductors like Si, Ge etc., N_C is greater than N_V, but for III-V compound semiconductors like InP, GaAs, GaP etc., the condition is reversed. So it has been found that when heterojunctions are formed between III-V compound semiconductors and other elements like Si or Ge, the product of respective carrier mobility and density of states and hence dark current is larger for p on n structures than for n on p structures. However, the above mentioned condition is reversed when heterojunction is formed between two III-V semiconductors and considerable improvement in conversion efficiency can be achieved if p on n structure is used instead of n on p structure. These facts reveal that due consideration should be given in case of choosing the band gaps of n and p type materials forming heterojunction solar cells. The results presented in chapter 3 show that the efficiency of a n-InP/p-GaP heterojunction solar cell is higher than p-InP/n-GaP cell by 19 %, where as the magnitude of improvement achieved by interchanging the n and p type materials of GaP/GaAs p-n heterojunction structures is around 13%. So it can be concluded that when p-n heterojunction is formed between two III-V compound semiconductors, p-type material

should have higher band gap than *n*-type material to achieve higher conversion efficiency.

5.1.2 Modification of Heteroface Solar Cells

It has been reported that conversion efficiency of a *p-n* homojunction solar cell can be improved by adding a layer of high band gap material to it [11-12]. This structure is known as 'heteroface' solar cell. The high band gap material is used as window layer which absorbs the high energy photons and allows the photons with low quantum energy to pass through and be absorbed by low band gap homojunction material. The window layer also decrease dark current and hence increase the open circuit voltage by providing higher potential barrier to either electrons or holes. Since electrons have higher mobility than holes, practically fabricated heteroface structures use a high band gap *p*-type material to suppress the electron component of dark current [12]. This work has presented a modification to the heteroface solar cells to achieve even higher conversion efficiency. It has been shown in chapter 4 that if, instead of a *p-n* homojunction, the high band gap window layer is added to a *p-n* heterojunction, the efficiency is increased significantly. In case of this proposed structure, photoresponse and hence the short circuit current density is increased significantly due to the use of *p-n* heterojunction instead of homojunction. As a result the maximum power output is also improved as compared to heteroface structures. The open circuit voltage of such structures can be increased by increasing the energy gaps of both top and window layer materials, as shown in figure 6 of chapter 4. Finally, some comparative results have been presented (table 4.1 of chapter 4) which clearly reveal that the proposed *n*-GaAs/*p*-Si/*p*-Al$_x$Ga$_{1-x}$As structure has improved photoresponse i.e. short circuit current density and efficiency as compared with reported heteroface solar cell of *n*-GaAs/*p*-GaAs/*p*-Al$_x$Ga$_{1-x}$As structure [11-12] and *n*-Al$_x$Ga$_{1-x}$As *n*-GaAs/*p*-GaAs/*p*-Al$_x$Ga$_{1-x}$As. The later structure mentioned above has two window layers of both *n* and *p* type materials added to *n* and *p* type layers of a *p-n* homojunction. This structure has efficiency better than the heteroface structure due to its higher open circuit voltage achieved by double window layer. It has been shown in table 4.1 of chapter 4 that proposed *n*-GaAs/*p*-Si/*p*-Al$_x$Ga$_{1-x}$As structure has 18% higher conversion

efficiency as compared to reported n-GaAs/p-GaAs/p-Al$_x$Ga$_{1-x}$As heteroface solar cells [11-12].

5.2 Limitations

In the following, the limitations of the work presented in this thesis has been discussed:

1. In the analysis presented here, it has been assumed that all photons having quantum energy higher than the band gap of solar cell material are absorbed and create electron hole pairs. But it is highly unlikely that all the photons absorbed will contribute to short circuit current. As the short circuit current density of all the structures have been calculated based on this assumption, they may be different from the practical values if the structures are practically fabricated.

2. In determining the values of dark current and hence efficiencies for various structures, the values of electron and hole mobility as a minority carrier should have been used. But the data available in the published literatures mainly give the majority carrier mobility as a function of majority carrier concentration [27]. The techniques for measuring minority carrier mobility is not straightforward, and consequently, their data are scarce and limited only to some extensively studied semiconductors like Si and GaAs. Therefore in many cases of this work, minority carrier mobility has been assumed to equal to the majority carrier mobility. This assumption may introduce some error, since the variation of minority carrier mobility with both doping density and temperature have been reported to be somewhat different from that of majority carrier mobility [27-28].

3. In deriving the current voltage relations for the structures presented here, the quasi Fermi levels for electrons and holes have been assumed to be flat across the barrier region. This assumption, known as quasi-equilibrium assumption [9], is not strictly correct as the quasi-Fermi levels must have some slope in this region [9].

5.3 Suggestions for Further Work

Based on the limitations discussed above, following works can be carried out in future:

1. The photocurrent and hence short circuit current should be obtained by calculating the generation rate of electron-hole as a function of distance from the semiconductor surface and wavelength of the incident photon [4]:

$$G(x, \lambda) = \alpha (\lambda) F (\lambda) [1 - R (\lambda)] \exp [-\alpha (\lambda) x] \qquad (5.1)$$

where $\alpha (\lambda)$ is the absorption coefficient, $F (\lambda)$ is the number of incident photons/ cm^2/ s per unit bandwidth and $R (\lambda)$ is the fraction of photons reflected from the surface. The variation of absorption coefficient with wave length is different for different materials. So a comparative study of short circuit current density can be carried out to find the materials and structure having best spectral response. Also the effect of the widths of several layers of different structures on short circuit current density and hence efficiency can be studied to design the optimum widths.

2. Research can be carried out to get the exact values of minority carrier mobility as a function of doping density for different materials.

3. Rigorous numerical calculation can be carried out to get the exact variation of quasi Fermi levels for electrons and holes under shinning conditions.

REFERENCES:

[1] M.A. Green, "Photovoltaics: coming of age," in *Conference Record, 21st IEEE Photovoltaic Specialist Conference*, Orlando, May 1990, *IEEE publ. no. 90CH2838-1*, p.1.

[2] D.M. Chapin, C.S. Fuller, G.L. Pearson, "A new silicon *p-n* junction photocell for converting solar radiation into electrical power," *J.Appl. Phys.* 8, 676 ,1954.

[3] M.A. Green, "Solar Cells," in *Modern Semiconductor Device Physics*, edited by S.M.Sze, p. 473, John Wiley & Sons, 1998.

[4] S.M. Sze, "Physics of Semiconductor Devices," *2nd ed., Wiley, Newyork*, 1981 (chapter 14 in particular).

[5] Masafumi Yamaguchi, Antonio Luque, "High Efficiency and High Concentration in Photovoltaics", *IEEE Trans. on Electron Devices*, vol. 46, no. 10, p. 2139, October 1999.

[6] Jenny Nelson, "Solar Cell Efficiency-Routes to Increasing the Limiting Efficiency of Solar Cells,"*Sci-Notes: Solar Energy,*,vol 2, no.2, 2002.

[7] C. H. Henry, "Limiting efficiencies of ideal single and multiple energy gap terrestrial solar cells", *J. Appl. Phys*, pp. 4494-4500, vol. 51, no. 8, 1980.

[8] J. Mandalkorn and J.H. Lamneck, "Simplified Fabrication of Back Surface Electric Field Silicon cells and Novel Characteristics of Such Cells," *Conf. Rec. 9th IEEE Photovoltaic Spec. Conf.*, IEEE, New York, p. 66, 1972.

[9] S.J. Fonash, "Solar Cell device Physics," *Academic Press Inc.*, 1981.

[10] John C. C. Fan, Carl O. Bozler, R.L. Chapman, "Simplified fabrication of GaAs homojunction solar cells with increased conversion efficiencies," *Appl Phys Lett.*, vol. 32, no. 6, p.492, March 1978.

[11] H.J. Hovel and J.M. Woodall, "$Ga_{1-x}Al_xAs$-GaAs *p-p-n* Heterojunction Solar Cells," *J. Electrochem. Soc.*, 120,1246, 1973.

[12] J.M. Woodall and H.J. Hovel, " An isothermal etchback-regrowth method for high efficiency $Ga_{1-x}Al_xAs$-GaAs solar cells," *Appl Phys Lett.*, vol. 30, no. 9, p.492, May 1977.

[13] C. Algora, E. Ortiz, I. Rey-Stolle, V. Diaz, R.Pena, V.M Andreev, V.P. Khvostikov, V.D. Rumyantsev, "A GaAs Solar Cells with an efficiency of 26.2% at 1000suns and 25.0% at 2000 suns," *IEEE Trans. On Electron devices,* vol. 48, no. 5, May 2000.

[14] H.J. Hovel, "Semiconductors and Semimetals," *Academic Press, New York*, vol.11, 1975.

[15] R.Meyer, A.Metz, M.Grauvogol, R.Hezel, "A Novel Type of MIS Inversion-Layer Silicon Solar Cell for Very High Efficiencies," *presented in the 2nd World Conf. on Photovoltaic Solar Energy Conversion,* Vienna, 1998.

[16] D. L. Feucht, "Heterojunction in Photovoltaic Devices", *J. Vac. Sci. Technol.*, Vol 14, pp.57, 1977.

[17] P. V. Meyers, R.W. Birkmire, "The future of CdTe Photovoltaics", *Progr. Photovol.* ,vol 3, pp 393, 1995.

[18] J. L. Shay, S. Wagner, H. M. Kasper, "Efficient $CuInSe_2$/CdS solar cells", *Appl Phys Lett.*, pp 89 , Vol 27, 1975.

[19] J. Wu, W. Walukiewicz, W. Shan, K. M. Yu, J. W. Ager , E. E. Haller, Hai Lu, W. J. schaff, "Unusual properties of the fundamental band gap of InN", *Appl Phys Lett.*, May 2002.

[20] R. W. Peng, M. Mazzer, K. W. J. Barnham, "Efficiency enhancement of ideal photovoltaic solarcells by photonic excitations in multi-intermediate band structures", *Appl Phys Lett.*, pp770-772 , Vol 83, 2003.

[21] W. Shockley and H.J. Queisser, "Detailed Balance limit of efficiency of *p-n* junction solar cells," *J. Appl Phys,* 32, 510, 1961.

[22] J.E. Parott, "Radiative recombination and photon recycling in photovoltaic solar cells," *solar Energy Mater. Solar Cells,*30,221,1993.

[23] J. J. Loferski, "Theoretical considerations governing the choice of the optimum semiconductor for photovoltaic solar energy conversion," *J. Appl Phys,* 27, 777, 1956

[24] R. L. Anderson, "Experiments on Ge-GaAs Heterojunctions," *Solid-State Electronic,* vol. 5, pp. 341-351,1962.

[25] M. Shur, "Physics of Semiconductor Devices," *Prentice-Hall, Inc. N.J., U.S.A,* 1990.

[26] A. Ahmed. Pavel and M. Rezwan Khan, "Exploitation of density of states and mobility difference between holes and electrons for high efficiency solar cells," *WSEAS Tran. on Electronics*, vol. 1, issue 1, pp. 56-59, Jan. 2004.

[27] M. Sotoodeh, A.H. Khalid, A.A. Rezazadeh, "Empirical low field mobility model for III-V compounds applicable in device simulation codes," *J. Appl. Phys*, vol. 87, no. 6, pp. 2890-2899, March 2000.

[28] Mark. E. Law, M. Liang and Dorotha E. Burk, "Self Consistent Model of Minority-Carrier lifetime, Diffussion length and Mobility," *IEEE Electron Device Lett.*, vol. 12, no. 8, pp 401-403, Aug. 1991.

[29] P.K. Basu, S.N. Singh, N.K. Arora and B.C. Chakravarty, "A New Method of Determination of Minority carrier Diffussion Length in the Base Region of Silicon Solar Cells," *IEEE Tran. on Electron device*, vol. 41, no. 3, pp 367-372, March 1994.

99 116

Appendix A

Properties of Ge, Si, InP, GaAs and GaP at 300 K used for calculation

Semi-conductors	Bandgap (eV)	Effective density of sates in conduction band, N_C (cm^{-3})	Effective density of sates in valence band, N_V (cm^{-3})	Mobility (cm^2/V-S)		Diffusion length (cm)	
				Electron	Hole	Electron	Hole
Ge	0.66	1.04×10^{19}	6×10^{18}	3000	900	0.0032	0.0022
Si	1.12	2.80×10^{19}	1.04×10^{19}	800	350	0.02	0.009
InP	1.35	5.70×10^{17}	1.10×10^{19}	3500	125	0.001	0.00041
GaAs	1.42	4.70×10^{17}	7×10^{18}	4500	270	0.0015	0.00032
GaP	2.26	1.80×10^{19}	1.90×10^{19}	150	140	0.000016	0.000016

- Both acceptor and donor doping density (N_A and N_D) has been assumed to be 10^{17} cm^{-3} in calculating the mobility values.

Appendix B

MATLAB Program to calculate built in potential and to generate *J-V* and *P-V* curves for *p*-on-*n* and *n*-on-*p* heterojunction structure

```
%generating J-V, P-V curves and calculating Vd

%values used
q=1.6e-19;kt=.026;

% optical current as a function of  smaller band gap
eg=1.42;
jop=(0.7181.*eg.^5-8.2694.*eg.^4+35.5250.*eg.^3-
61.8203.*eg.^2+10.6480.*eg.^1+61.7508)

% for Egp>Egn i.e p-on-n
%n is GaAs and p is GaP
un=150;up=270;
ln=15.8e-6;lp=32.1e-5;
Dp=kt*up;Dn=kt*un;
nd=1e17; na=1e17;
ncn=4.7e17;nvp=1.9e19;%Nc of GaAs & Nv of GaP
egp=2.26;
egn=1.42;
x=ncn*nvp;
Vd=eg+kt*log(na*nd/x)
jsp=1e3*q*(Dp/lp)*(x/nd)*exp(-1.*egn/kt);
jsn=1e3*q*(Dn/ln)*(x/na).*exp(-1.*egp/kt);
js=jsp+jsn;
voc=kt*log(1+jop./js);
v=0:.01:1.2;
j=jop-js.*(exp(v/kt)-1);
p=j.*v;
plot(v,j,'r')
hold on
plot(v,p,'r')


% for Egn>Egp i.e n-on-p (existing)
% n is GaP & p is GaAs
un=4500;up=140;
ln=14.8e-4;lp=16e-6;
Dp=kt*up;Dn=kt*un;
nd=1e17; na=1e17;
ncn=1.8e19;nvp=7e18;
x=ncn*nvp;
Vd=eg+kt*log(na*nd/x)
egn=2.26;
egp=1.42;
jsp=1e3*q*(Dp/lp)*(x/nd)*exp(-1.*egn/kt);
jsn=1e3*q*(Dn/ln)*(x/na).*exp(-1.*egp/kt);
```

```
js=jsp+jsn;
voc=kt*log(1+jop./js);
hold on
v=0:.01:1.2;
j=jop-js.*(exp(v/kt)-1);
p=j.*v;
plot(v,j,'b')
hold on
plot(v,p,'b')
```

- for heterojunction formed by other materials values of different parameters have to be changed

Appendix C

MATLAB Program for *p-n* homojunction of GaAs structure

```
%values used
q=1.6e-19;kt=.026;

% optical current as a function of  smaller band gap
eg=1.42;
jop=(0.7181.*eg.^5-8.2694.*eg.^4+35.5250.*eg.^3-
61.8203.*eg.^2+10.6480.*eg.^1+61.7508)

% for Egp>Egn i.e p-on-n (our proposal)
%n is Si and p is GaAs
%calculating thermal current
un=4500;up=270;
Dp=kt*up;Dn=kt*un;
nd=1e17; na=1e17;
ln=14.8e-4;lp=32.1e-5;
ncn=4.7e17;nvp=7e18;%Nc og Ge & Nv of GaAs
egp=1.42;
egn=1.42;
x=ncn*nvp;
Vd=eg+kt*log(na*nd/x);
jsp=1e3*q*(Dp/lp)*(x/nd)*exp(-1.*egn/kt);
jsn=1e3*q*(Dn/ln)*(x/na).*exp(-1.*egp/kt);
js=jsp+jsn
voc=kt*log(1+jop./js)
hold on
v=0:.01:1.12;
j=jop-js.*(exp(v/kt)-1);
p=j.*v;
plot(v,j,'r')
hold on
plot(v,p,'r')
```

Appendix D

MATLAB Program for n-GaAs/p-GaAs/p-Al$_x$Ga$_{1-x}$As heteroface structure

```
%values used
q=1.6e-19;kt=.026;

% optical current as.a function of  smaller band gap
eg=0:.01:4;
jo=(0.7181.*eg.^5-8.2694.*eg.^4+35.5250.*eg.^3-
61.8203.*eg.^2+10.6480.*eg.^1+61.7508);
pin= trapz(eg,jo)

% for homojumction of GaAs and then a reflector
%calculating thermal current
eg=1.42;
jop=(0.7181.*eg.^5-8.2694.*eg.^4+35.5250.*eg.^3-
61.8203.*eg.^2+10.6480.*eg.^1+61.7508)
un=4500;up=280;un1=280;
Dp=kt*up;Dn=kt*un;Dn1=kt*un1;
ln=14.8e-4;lp=32.1e-5;ln1=14.8e-4;
nd=1e17; na=1e17;
ncn=4.7e17;nvp=7e18;
egn=1.42;egp=1.42;
x=ncn*nvp;
npo=x*exp(-1*egp/kt)/na;
pno=x*exp(-1*egp/kt)/nd;
eg1=1.99;nc1=1.74e19;nv1=1.235e19; %parameters for AlGaAs
npo1=(nc1*nv1)*exp(-1*eg1/kt)/na;
r=.01;%w/Ln
jsp=1e3*q*(Dp/lp)*pno
jsn=1e3*q*((Dn*2*npo./(ln.*((2./r)-1)))+Dn1*npo1/ln1)
js=(jsp+jsn);
voc_homo=kt*log(1+jop./js)
v=0:.01:1.5;
j=jop-(jsp+jsn)*(exp(v/kt)-1);
plot(v,j,'g')
hold on
p=j.*v;
plot(v,p,'g')
```

Appendix E

MATLAB Program for n-Al$_x$Ga$_{1-x}$As/n-GaAs/p-GaAS/p-Al$_x$Ga$_{1-x}$As structure

```
%values used
q=1.6e-19;kt=.026;

% optical current as a function of  smaller band gap
eg=0:.01:4;
jo=(0.7181.*eg.^5-8.2694.*eg.^4+35.5250.*eg.^3-
61.8203.*eg.^2+10.6480.*eg.^1+61.7508);
pin= trapz(eg,jo)

%calculating thermal current
eg=1.42;
jop=(0.7181.*eg.^5-8.2694.*eg.^4+35.5250.*eg.^3-
61.8203.*eg.^2+10.6480.*eg.^1+61.7508)
un=4500;up=280;un1=280;up1=70;
Dp=kt*up;Dn=kt*un;Dn1=kt*un1;Dp1=kt*up1;
ln=14.8e-4;lp=32.1e-5;ln1=14.8e-4;lp1=32.1e-5;
nd=1e17; na=1e17;
ncn=4.7e17;nvp=7e18;
egn=1.42;egp=1.42;
x=ncn*nvp;
npo=x*exp(-1*egp/kt)/na;
pno=x*exp(-1*egp/kt)/nd;
eg1=1.99;nc1=1.74e19;nv1=1.235e19; %parameters for AlGaAs
npo1=(nc1*nv1)*exp(-1*eg1/kt)/na;
pno1=(nc1*nv1)*exp(-1*eg1/kt)/nd;
r=.01;%w/Ln
jsp=1e3*q*((Dp*2*pno./(lp.*((2./r)-1)))+Dp1*pno1/lp1);
jsn=1e3*q*((Dn*2*npo./(ln.*((2./r)-1)))+Dn1*npo1/ln1);
js=(jsp+jsn);
voc_homo=kt*log(1+jop./js)
v=0:.01:1.5;
j=jop-(jsp+jsn)*(exp(v/kt)-1);
plot(v,j,'b')
hold on
p=j.*v;
plot(v,p,'b')
```

Appendix F

MATLAB Program for *n*-GaAs/*p*-Si/*p*-Al$_x$Ga$_{1-x}$As structure

```
%values used
q=1.6e-19;kt=.026;

% optical current as a function of   smaller band gap
eg=0:.01:4;
jo=(0.7181.*eg.^5-8.2694.*eg.^4+35.5250.*eg.^3-
61.8203.*eg.^2+10.6480.*eg.^1+61.7508);
pin= trapz(eg,jo)

% for heterojumction of Si & GaAs and then a reflector
%calculating thermal current
eg=1.12;
jop=(0.7181.*eg.^5-8.2694.*eg.^4+35.5250.*eg.^3-
61.8203.*eg.^2+10.6480.*eg.^1+61.7508)
un=800;up=280;un1=280;
Dp=kt*up;Dn=kt*un;Dn1=kt*un1;
ln=34e-4;lp=32.1e-5;ln1=14.8e-4;
nd=1e17; na=1e17;
ncn=4.7e17;nvp=1.04e19;
egn=1.42;egp=1.12;
x=ncn*nvp;
npo=x.*exp(-1.*egp/kt)/na;
pno=x*exp(-1.*egn/kt)/nd;
eg1=1.12:.01:1.99;ncl=1.74e19;nvl=1.235e19; %parameters for AlGaAs
npol=(ncl*nvl).*exp(-1*eg1/kt)/na;
r=.001;%w/Ln
jsp=1e3*q*(Dp/lp).*pno;
jsn=1e3*q.*((Dn*2.*npo./(ln.*((2./r)-1)))+Dn1.*npol/ln1);
js=(jsp+jsn);
voc_het=kt*log(1+jop./js);
subplot (2,1,2);plot(eg1,voc_het,'X')
hold on
```